이학박사 학위논문

# Electrical characterization of rectifying and photoswitching molecular devices

정류 분자 소자와 광스위칭 분자 소자의

전기적 특성 연구

2017 년 2 월

서울대학교 대학원

물리천문학부

김 동 구

# Electrical characterization of rectifying and photoswitching molecular devices

정류 분자 소자와 광스위칭 분자 소자의 전기적 특성 연구

지도 교수 이 탁 희

이 논문을 이학박사 학위논문으로 제출함

2017년 2월

서울대학교 대학원

물리천문학부

김 동 구

김동구의 이학박사 학위논문을 인준함

2017년 2월

위 원 장 홍 승 훈 (인)

부위원장 이 탁 희 (인)

위 원 김 대 식 (인)

위 원 홍 성 철 (인)

위 원 왕 건 욱 (인)

# Abstract

As one of the interesting research fields, the molecular electronics has been studied to be used as electronic device components such as rectifier, transistor, memories, and photoswitch. In particular, molecular self-assembled monolayer (SAM) can be used to a functional device structure due to several advantages such as low fabrication cost, high efficiency, less heat problem, and miniaturized junction size. However, the early day of molecular electronic devices had a problem of low device yield (typically less than 1 %) because of the electrical shorts that can occur as a result of the top electrode's penetration through the thin molecular layers. To solve this problem, several ways have been proposed. First, an intermediated protective layer composed of a conducting polymer, or graphene film have been introduced between the molecular layer and the top electrode. Or, top electrode has been directly transferred on the molecular layers. As a result, the yield of molecular electronic devices increased high (> 80 %) and the electrical properties of molecular devices were well maintained during a long period of operation.

With the development of high-yield molecular devices, it became possible to fabricate molecular devices even on flexible substrates. Our research group previously reported that alkanethiol molecular devices could be fabricated on flexible substrates with showing operative electrical properties under bending conditions. However, alkanethiol molecules are insulating and not suitable for real application because of the absence of potential device

functionality. Therefore, I started to fabricate functional molecular devices on flexible substrates. In this thesis study, I fabricated rectifying and photoswitching molecular devices on flexible substrates and studied the electrical properties under bent substrate conditions. First, ferrocene-alkanethiolate functional molecular devices showed asymmetric electrical characteristics on both rigid and flexible substrates. I observed asymmetric current-voltage behavior because of a redox process of ferrocene part of rectifying molecules although the current asymmetric ratio (~1.6) was rather low. The rectifying molecular devices were well maintained in the asymmetric electrical behaviors under bent conditions. Second, diarylethene molecules are known to have two electrical conductance states; a closed (high conductance) state or an open (low conductance) state can be created upon illumination with UV or visible light, respectively. These two electrical states were defined and fixed during the device fabrication with illuminations of either UV or visible light, and showed distinct current levels between the two states. However, the fabricated diarylethene molecular devices did not show reversible switching phenomena. Lastly, in order to demonstrate reversible photoswitching process, I fabricated and characterized diarylethene molecular devices by using reduced graphene oxide (rGO) as top electrode. The photoswitching molecular devices with rGO top electrode successfully exhibited two stabile electrical states with different current levels and with reversible photoswitching capability. This study has a promise towards functional molecular devices on flexible substrates.

**Keywords**: Molecular electronics, self-assembled monolayer, high yield molecular devices, ferrocene-alknaethiol, rectification ratio, redox process, isomerization, diarylethene, reduced graphene oxide, flexible electronics

**Student number: 2010-20358**

# Contents

# List of Figures

## Chapter 1.



## Chapter 2.

## Chapter 3.

## Chapter 4.

# List of Tables

# Chapter 1
# Introduction

## 1.1 Overview molecular electronics

The modern industrial technology based on complementary metal-oxide semiconductor (CMOS) has been developed rapidly and has provided enormous convenience to modern society. However, such this technology has reached the technical barriers due to the quantum tunneling effect of nano-scale device size. In addition, the fabrication cost of device will increase incredibility. To overcome these problems facing modern technology, molecular electronic devices have been studied as one of areas with potential. Over the past several decades, molecular electronic field have been investigated a single molecules or self-assembled monolayer (SAM) field which are utilized molecules as devices component [1-23]. In the particular advantages aspect of SAM can generate the fabrication of a single or many molecular devices on both $SiO_2$/Si substrates and flexible platform. Especially, part of a single molecular device can give the possibility of investigation of charge transport of molecule itself through electromigrated break junctions [24-28] and mechanical controlled break junction (MCBJ) [29-42].

Since A. Aviram and Ratnet proposed electron donor-acceptor molecule as a molecular diode in 1974 [43], molecular electronic devices have been widely studied for many research categories such as rectifier [44-53], switches [54-58], transistor [28, 59, 60], memories [61-65] and photoswitching [58, 66-73]. Furthermore, various devices platform designs have also been studied such as scanning probe microscope-based techniques [74-80], atomic force spectroscopy tip loading technique [81], crossed-wire tunnel junctions [45, 78, 82-84] and Hg drop junctions [85-92]. In addition, since SAM can be deposited on various surface materials such as Au [65-69], Ag [93-102], Cu [103-106], Pd [107-112], Pt [111], Ni [112-119] and Fe [120, 121], it can be also studied about the electrical properties of molecular layers combined with various materials. However, early molecular electronics are hardly practical because it has a very low devices yield owing to electrical short problem that may occur as a result of the top electrode particles penetration through the molecular layers [122-124]. To solve this electrical short problem, several attempts have been proposed, such as using intermediate protective layer composed of a conducting polymer [125-128], or graphene film [66, 129, 120 ] on molecular layer and direct metal transfer [131]. These methods have remarkably increased devices yield of molecular electronics.

With high yield device making approach, this thesis surveys the fabrication process of functional (rectifying, photoswitching) molecular devices on flexible substrates and investigate electrical characterization the

molecular devices under bending condition. The type of rectifying molecule has been studied asymmetry electrical characterization between positive and negative bias, photoswitching molecules has been studied isomerization property in which the two electrical conductance states changed reversible in both direction of each states. We also discuss the electrical characterization of the molecular devices on flexible substrates under mechanical deformation.

# 1.2 Langmuir-Blodgett Films

Langmuir-Blodgett films (L-B films) is the one of famous deposition methods for molecular layer from surface of liquid to solid substrates by using "Amphiphile" type molecules [6]. The origin of the L-B films is that Benjamin Franklin carried out first attempt when he dropped a layer of oil into pond [132]. After this trial, many scientists tried to make a molecular monolayer at the liquid surface [133-138] and two scientists, named Irving Langmuir, Katherine Blodgett, figured out the first systematic deposition method of amphiphile molecules at liquid surface [139-141]. In past times, although mercury and the other materials have been used by subphase ingredient, the mostly used subphase material in this day is water due to high surface tension (72.0 mN/m at 25 ℃) and safety.

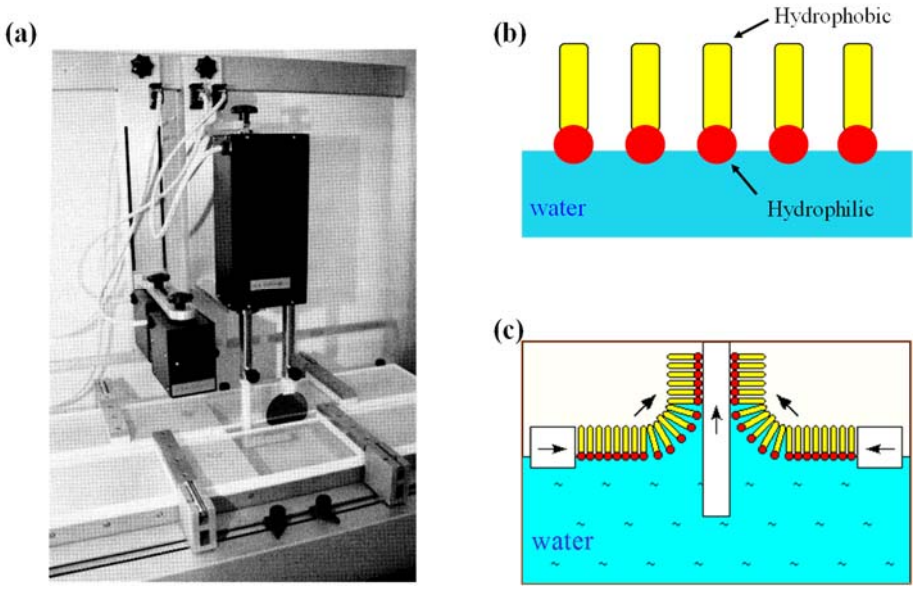


**Figure 1-1(a) The KSV 5000 (b) Alignment of amphiphile molecules on water surface (c) L-B films deposition on hydrophilic substrates**

Amphiphile type molecules is defined that molecule is made up head part of hydrophilic which means they like water and tail part of hydrophobic which means they are afraid of water. Carboxylic acid and fatty acid are typically amphiphile molecules. When this amphiphile molecular solutions is dropped at water surface and push on both side with barrier, amphilphile molecules are line up as figure 1-1-(b) (i.e. head part (hydrophilic) is headed for water direction while tail part (hydrophobic) is headed for opposite direction). And then, if the solid substrate is hydrophilic, the molecular layer is deposited by raising the substrates whereas if the solid substrates is hydrophobic, the layer is deposited by lowering substrates.

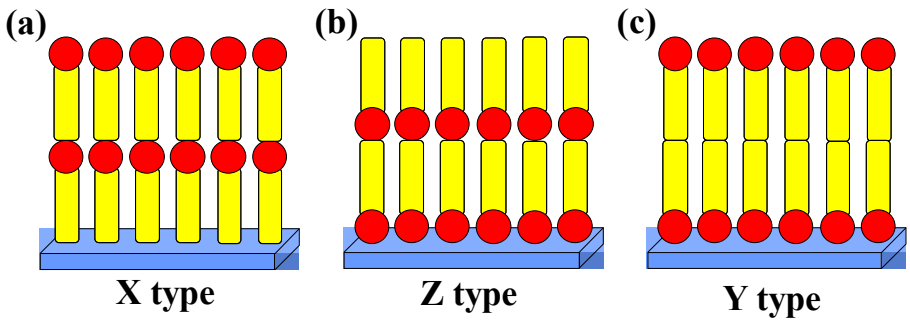


**Figure 1-2. Three types of Langmuir-Blodgett films (a) X type (b) Z type (c) Y type**

L-B films can be formed multi molecular layers on solid substrate. There are three kind of L-B multi layers film, X, Y, and Z type as shown figure 1-2. Among them, Y type L-B films is the most stable deposition mode due to interaction between each hydrophilic-hydrophilic or hydrophobic-hydrophobic, as figure 1-2-(c). In the X type case, hydrophobic substrate interacts with hydrophobic tail part during lowering the substrate at inside water and tail part interacts hydrophilic head part. However, since hydrophilic part and hydrophobic part are impossible to interaction each other, the tail part is terminated by a weak polar group (e.g. $–NO_2$). The rest type Z is opposite style compared X type L-B film, as shown figure 1-2-(b). The X type arrange molecular layer like tail-head-tail-head while Z type arrange molecular layer like head-tail-head-tail. The X and Y type are less stable than Y type due to interaction between hydrophilic and hydrophobic. Many equipment of surface analysis has been used to investigation and characterization of L-B films for instance surface-enhanced Raman spectroscopy (SERS) [142], surface

extended x-ray fine structure (SEXAFS) [143], near-edge x-ray absorption fine structure (NEXAFS) [144].

# 1.3 Self-assembled monolayers

Self-assembled monolayers (SAM) are defined that molecular monolayers are formed spontaneously chemisorption between molecular head group and appropriate surface of substrate as shown figure 1-3. Previously, Langmuir-Blodgett films (L-B films) is one of good methods for deposition of molecular layer on substrates, but there is potential problem that molecular layer is non-uniform due to a short contact time between subphase water and substrate. In addition, because of physisorption between molecular monolayer and substrates, the layer is very weak from outside impact and contaminant. On the other hand, SA methods have a long contact time (24 ~ 48 h) by immersion of a substrates into the molecular solutions. In addition, chemisorption between thiol and Au is strongly binding. Because of this advantage of SAM methods, this process gives uniformly and stability. The thiol can be chemisorption on appropriate substrates materials [65-69, 93-121]. Among them alknethiols SAM formed on Au (111) are well known systems and have been widely studied molecular structure and electrical characterization [6, 145, 146]. This thesis focus on functional molecular monolayer on flexible substrates like ferrocene-alknaethiol [147], photoswitching diarylethene [68, 69].

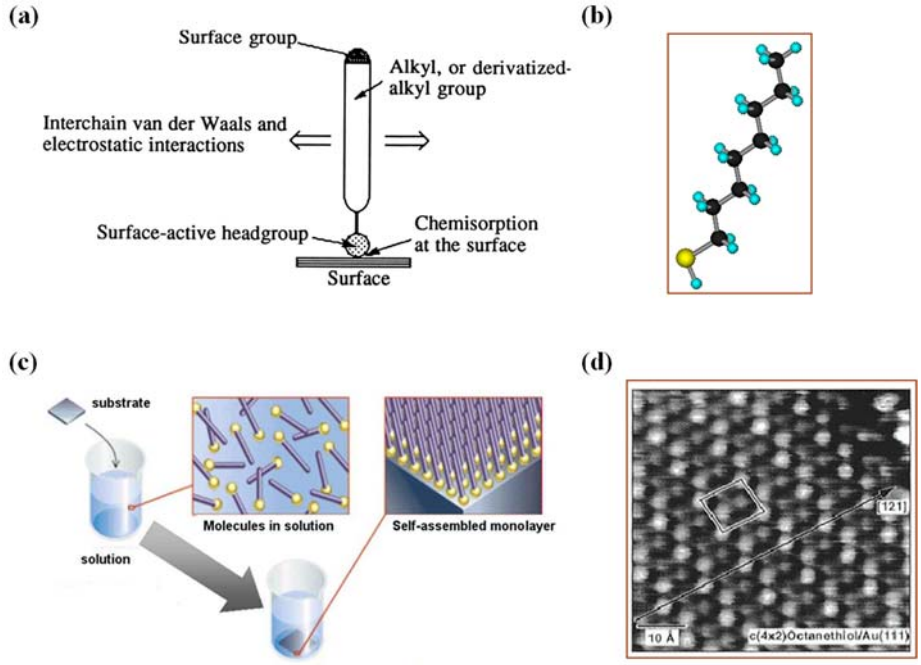


**Figure 1-3. (a) A schematic view of the forces in a self-assembled monolayer (b) Octanethiol (c) Process of self-assembled monolayer (d) STM image**

A alknaethiol molecule is a thiol-terminated n-alkyl chain molecular organization i.e. $[CH_3(CH_2)_{n-1}SH$ [6]. This molecule consists of three parts that are surface-active headgroup, hydrcabron cahin of body and terminal end group. The first molecular part, (SH) thiol group, is surface-active headgroup that is strongly chemisorption with metallic surface for instance ~50 kcal/mol for S-Au bond [6]. The second part, $((CH_2)_{n-1})$ alkyl chain, is hydrocarbon chain of body which maintain standing up phase through van der Walls interaction between neighborhood molecules as shown figure 1-3-(a). The alknaethiols case standing up 30 degrade angle of vertical direction from ground. The rest part, methyl ($CH_3$) group, is terminal group that can be synthesized functional

group like ferrocene [147], azobenzen [66, 67, 73]. Figure 1-3-(b) show a chemical structure of octanethiol, a type of alkanehtiol. The process of alkanethiol SAM is shown as figure 1-3-(c), where gold surface substrates is immersed on molecular solutions and after a period time the monolayer is formed spontaneously on gold surface with highly ordered and closed packed molecular layer following chemical reaction process.

$$\mathbf{RS\text{-}H + Au \rightarrow RS\text{-}Au + 0.5H_2}$$

where R is backbone of molecules. At the begging time of this chemisorption process take very rapidly time within minutes and give ~90 % film thickness [6, 146]. And then, slow process takes hours to transition SAM layers from lay-down phase to ordered standing-up phase and form uniformly crystallization of the alkyl chains. The uniformly molecular monolayer is confirmed by various surface analytical tool such as infrared (IR) and Fourier transform infrared (FTIR) spectroscopy [148, 140], X-ray photoelectron spectroscopy (XPS) [150], Raman spectroscopy [151], scanning tunneling microscopy (STM) [152] etc.

# 1.4 Low devices problems

For breakthrough of molecular deposition methods like L-B films [6, 139-141] and self-assembled methods [68, 69, 73, 122-131], many scientists have tried to fabricate and study electrical characterization of molecular devices. However, early molecular devices had seriously problem about low yield (less

than ~ 1%) due to penetrate top electrode particle between neighborhood molecules [122-124]. Because the thermally evaporated top electrode particle had enough thermal kinetic energy to penetrate molecular layer, nearly all molecular devices exhibited electrical short phenomena as shown Table 1. In particular, alkanethiols, which is known as an insulating molecule, have been made molecular electronic devices and its electrical properties have been studied extensively [122-131]. For statistical analysis these electrical short problem, our group have been fabricated a large number of pure metal-molecular-metal structure and analyzed them by using Gaussian distribution. Figure 1-4 shows a schematic diagram of a metal–alkanethiol–metal junction device and molecular structures of octanedithiol (DC8) and octanethiol (C8).

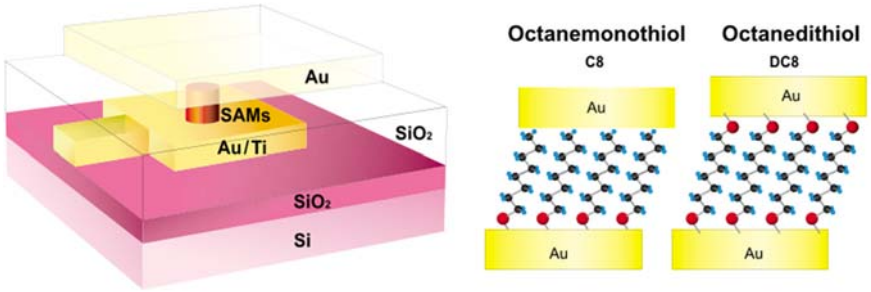


**Figure 1-4. A Schematic of micro holes type molecular devices on rigid substrates and generally metal-molecular-metal structure**

As mentioned above, the low yield devices problem of molecular devices happened due to electrical shorting phenomenon. When “working” devices can be defined as devices having nonlinear I-V characterization and not being electrical open and short, our group represented 11744 electrical shorts, 392 fabrications failure and 1103 electrical open, 156 working devices among

13440 total number of molecular devices, respectively (Table 1). The number of 11744 electrical shorts phenomena among total number of devices demonstrated that top electrode connected bottom electrode due to penetrate top electrode materials.

| | No. of fabricated devices | Fab. failure | Short | Open | Nonworking | Working | | | Device yield |
|---|---|---|---|---|---|---|---|---|---|
| | | | | | | C8 | C12 | C16 | |
| Monothiol | 13440 (100%) | 392 (2.9%) | 11744 (87.4%) | 1103 (8.2%) | 45 (0.3%) | 63 (1.41%) | 33 (0.69%) | 60 (1.44%) | 156 (1.2%) |
| | | | | | | DC8 | DC9 | DC10 | |
| Dithiol | 14400 (100%) | 472 (3.28%) | 12340 (85.7%) | 1252 (8.69%) | 65 (0.45%) | 84 (1.75%) | 94 (1.96%) | 93 (1.94%) | 271 (1.9%) |

**Table 1. Summary of yield of fabricated molecular devices**

To overcome this problem, several ideas have been proposed, such as using intermediate protective layer composed of a conducting polymer [125-128], or graphene [129, 130] film between the molecular layer and the top electrode. In addition, methods of directly top electrode transport have been studied [131]. These attempts have greatly increased the yield of the molecular devices.

# 1.5 Intermediate protective layer

## 1.5.1. Conducting polymer; PEDOT:PSS

The intermediate protective conducting layer have been widely studied for solving the penetration top electrode between molecular layers. Among

them PEDOT:PSS is one of good conducting polymer because of similar work function compared gold and adjusting electrical conductivity through doping. Figure 1-5-(a) show the fabrication process of a large-area molecular devices with PEDOT:PSS intermediate protective layers [125]. After vapor deposition gold electrode on a silicon wafer, SAM hole is made by photolithography. The device is immersed into molecular solution for SAM deposition at there. To get high yield molecular devices, conducting polymer PEDOT:PSS is spin-coated on SAM layer. Finally, the junctions is completed by deposition gold top electrode, which act reactive ion etching (R.I.E) to remove residual PEDOT:PSS.

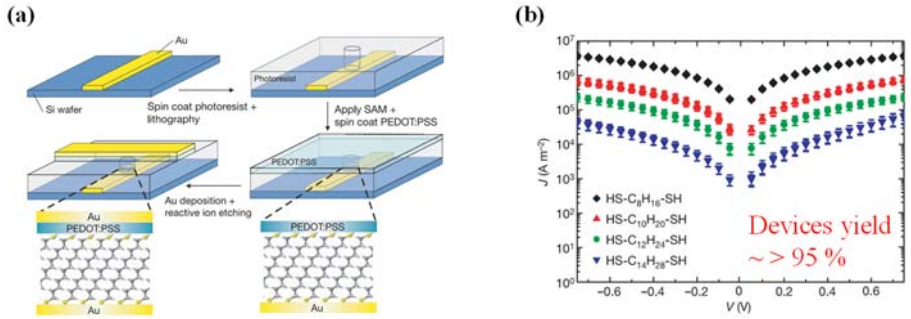


**Figure 1-5. (a) Fabrication process of large-area molecular devices with PEDOT:PSS (b) The J-V plot of 1,8-octanedithiol, 1,10-decanedithiol, 1,12-dodecanedithiol and 1,14-tetradecanedithiol**

Due to a large HOMO-LUMO gap of alknaethiol (~8 eV) [153, 154], the dominant charge transport mechanism of these molecular devices is the tunneling effect, which can be evidence that the current density decrease exponentially with depending molecular length in figure 1-5-(b) by following equation $J \propto J_0 \exp(-\beta_0 d)$ where $\beta_0$ is the decay coefficient and d is tunneling

length which indicates that the current depends on the barrier width exponentially [153, 156]. When the compared with conventional metal-molecules-metal structure, the current density characteristics looks like same and devices yield is remarkably improved (more than ~90 %) [125].

## 1.5.2. Graphene multilayers transfer

To overcome low devices yield, our group have studied to use graphene layer as intermediate protective layer [129]. Graphene is two-dimensional material, which forms an atomic scale hexagonal lattice with strong carbon-carbon covalently bond. In addition, it has good conductivity, electrical properties, chemical stability and mechanical material properties [157-160]. Because graphene layer is directly transferred on SAM layer, it can reduce the possibility of damage by spin-coating PEDOT:PSS. For these reasons, graphene sheet is greatly one of candidate as intermediate protective layer.

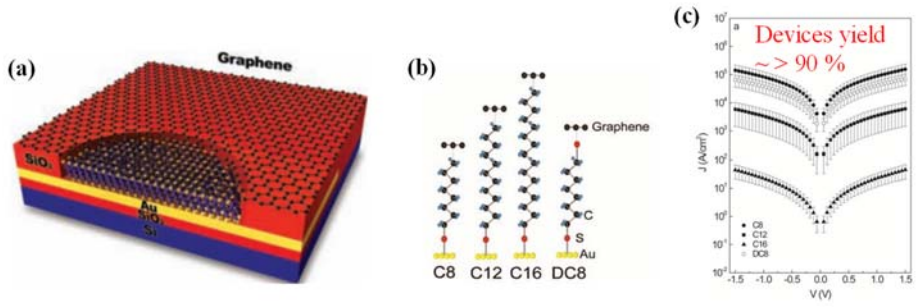


**Figure 1-6. Schematic of molecular devices with graphene protective layer (b) Chemical structure of octanethiol, dodecanethiol, hexadecanethiol and octanedithiol (c) The J-V plots of all molecular devices**

Our group have fabricated three types of molecules of different lengths that are octanethiol (for short C8), dodecanethiol (C12), hexadecanethiol (C16) and two different kind of molecules that are octanethiol (C8), octanedithiol (DC8) as shown figure 1-6-(b). According to above equation $J \propto J_0 \exp(-\beta_0 d)$, the current density of each molecular devices in figure1-6- (c) also varies according to the different lengths of molecules, like PEDOT:PSS/Au structure. In case of thiol and dithiol, the reason why conductivity C8 is higher than DC8 is due to physical contact between molecules and graphene. That is, the effective tunneling length of DC8 becomes longer by sulfur atoms of dithiol.

| | | | | | | Working (Device yield) | | | |
|---|---|---|---|---|---|---|---|---|---|
| Device type | Molecule | # of fabricated devices | Fab. Failure | Short | Nonworking | DC8 | C8 | C12 | C16 |
| Graphene-Based | Monothiol | 919 | - | 73 | 70 | | 240 (87.91%) | 278 (84.50%) | 253 (80.50%) |
| | Dithiol | 263 | - | 1 | 4 | 258 (98.1%) | | | |
| Au/molecule/Au | Monothiol | 13440 | 392 | 11744 | 45 | | 63 (1.41 %) | 33 (0.69 %) | 60 (1.44 %) |
| | Dithiol | 4800 | 192 | 4080 | 16 | 84 (1.75 %) | | | |
| PEDOT:PSS-Based | Dithiol | 128 | 4 | 35 | 15 | 74 (58 %) | | | |

**Table 2. Summary of yield of fabricated molecular devices with graphene layer**

In term of devices yield, molecular devices with graphene multi layers show high yield of over 90%. When compared to pure metal-molecules-metal [122, 123], it shows a largely high yield devices and it also shows good performance of devices compared with PEDOT:PSS protective layer.

## 1.5.3. Direct metal transfer methods

By new approaching methods, direct top electrode metal transfer [131] on SAM layer is new method for fabricating high yield molecular devices, similar

to graphene multilayers transfer on SAM. In order to top electrode capable transfer, top material is deposited at dummy substrate ($SiO_2$/Si) with low deposition rate for getting smooth surface to be contacted with SAM layer. Next, the PMMA was spin-coated onto the dummy substrate to support the Au electrodes that can be damaged while the film is being detached from the substrate. To detach the top electrode from dummy substrate, it is immersed at etching solutions potassium hydroxide (KOH) for being etched the $SiO_2$ layers on the dummy substrates. After finishing etching process, top electrode can be transferred on SAM layer as shown figure 1-7-(a) [131]. For comparison electrical properties of previous molecular devices, alkanethiol species, figure 1-7-(b), used in this new method were octanethiol (denoted as C8), dodecanethiol (C12) and hexadecanethiol (C16).

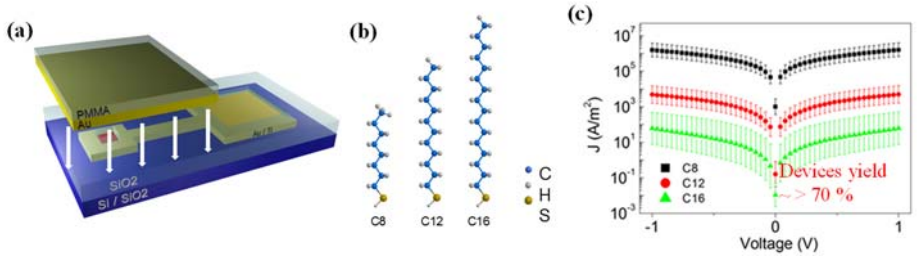


**Figure 1-7. (a) Illustration of metal transfer top electrode (b) Chemical structure of octanethiol, dodecanethiol and hexadecanethiol (c) The J-V plots of all molecular devices**

As previously reported, the dominant charge transport mechanism through alkanethiolates is known as off-resonant tunneling [28, 125]. Therefore, the current density depends on the exponentially molecular length. In figure 1-7-(c), the current density-voltage characteristics was exponentially dependent on the molecular length, like PEDOT:PSS/Au and graphene multilayer structure.

In addition, while conventional molecular devices of metal-molecules-metal type was very low yield due to penetrate gold particles with thermally kinetic energy between molecular layer, the metal transfer methods show more than ~70 % yield each C8, C12, C16, respectively.

# Chapter 2
# Rectifying molecular devices

## 2.1 Introduction

With the aim of modern science and technology to be able to wear and attach to human body, it is necessary to study of characterization, maintenance, stability, reliability of molecular electronics on flexible substrates. Flexible substrate research in modern technology include electronic circuits [161], sensors [162], displays [163], solar cells [164] and bioelectronics devices [165]. As with this development direction, our group tried to fabricate molecular devices on flexible substrates and study electrical characterization of the devices for ultimate aim of fabrication molecular logic circuits [128]. Figure 2-1-(a) shows the alknaethiol molecular devices on flexible substrates with consisting of schematic, optical image, SEM, TEM and molecular structure. Our group selected three types of alknaethiol molecules with different length; Octanethiol (as denoted C8), Decanethiol (C10), Dodecanethiol (C12). Previously reported about main mechanism of alknaethiol [28, 125],

alknaethiol molecular devices on flexible substrates showed the current density characteristics according to each molecular length. In addition, our group measured electrical characterization of the molecular devices under bending conditions that are different bending radii and a large number of repeated bending cycles in figure 2-1-(c), (d). Although our group have demonstrated that the molecular devices substrates were well implemented in flexible substrates and maintained good electrical properties under bending condition, these devices have difficult to apply into reality because alknaethiols lacks functionality as a simple insulating type. For the real application of molecular devices, we need to fabricate functional molecular devices on flexible substrates.

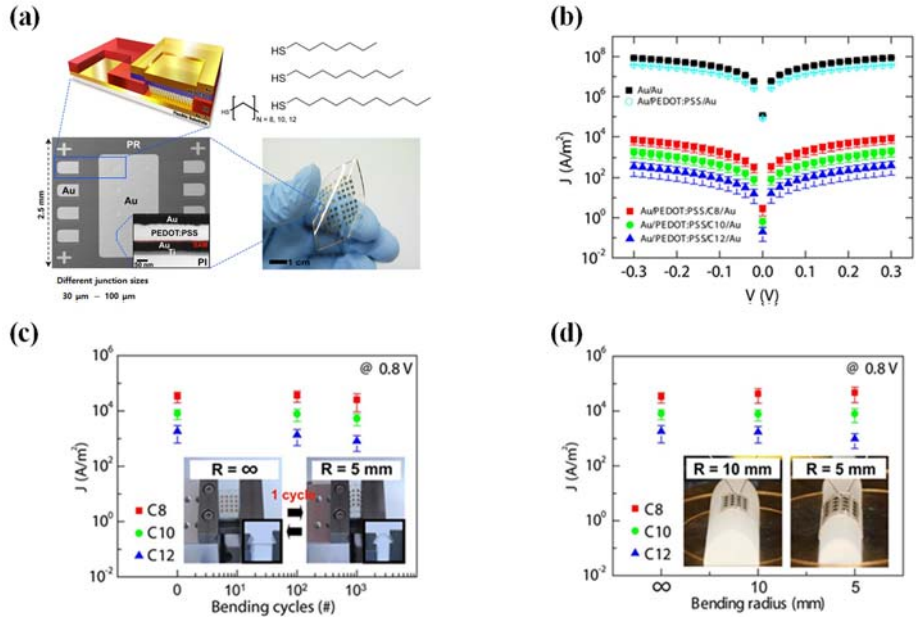


**Figure 2-1. . (a) Schematic of molecular devices on flexible substrates with illustration of junction, SEM, TEM, optical images and chemical structure (b) The J-V plots of all molecular devices (c), (d) The J value at +0.8 V under bending conditions**

SAM (self-assembled monolayer) method give possible to be used functional molecular group as devices component. Among them ferrocene is a typical rectifying molecule which consists of two cyclopentadienyl rings bound on opposite sides of a central metal atom ($Fe(C_5H_5)_2$)) and shows abnormal electrical characterization defined ratification ratio ($R \equiv |J(-1\ V)/J(+1\ V)|$) [51]. To represent rectifying behavior, the EGaIn (eutectic Gallium-Indium) technique [44, 48, 49] is very useful technology. This technique uses liquid type metal as a non-invasive top electrode that contact SAM layer deposited on template-stripped silver ($Ag^{TS}$) bottom electrode, ash shown figure 2-2-(a).

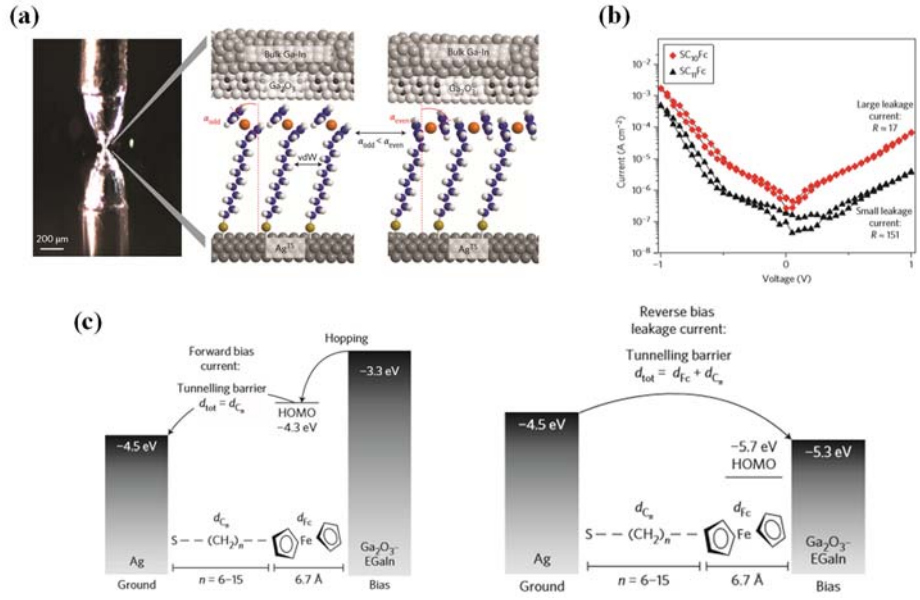


**Figure 2-2. (a) Optical image and schematic of ferrocene-alknaethiol junction with EGaIn electrode (b) The J-V plot of molecular junction (c) Energy diagram of -1 V and +1 V molecular junction**

Figure 2-2-(b) represent abnormal electrical characterization of ferrocene-alknaethiol junction with EGaIn top electrode. The rectification ration is about

10 to 100. The reason of this phenomenon is understood to locate of ferrocene's the highest occupied molecular orbital (HOMO) level, as shown figure 2-2-(c). With reverse bias (+1 V), HOMO level of ferrocene lies below Fermi levels of two electrodes which mean that charge cannot be injected into HOMO level. At forward bias (-1 V), molecular HOMO level lies between Fermi level of both electrodes which mean charge can be injected into HOMO level. Because of molecular HOMO level, tunneling width of both polarities is determined as $d_{tot,reverse}=d_{Fc}$(Fc units) + $d_{Cn}$(alkyl spacer) or $d_{tot,forward}=d_{Cn}$, respectively. This different tunneling width results in the large observed current rectification ratio. However, since EGaIn type rectifying molecular junctions have possibility of stability and maintenance, we aimed to solve these problems by fabricating rectifying molecular in the form of devices.

- **Devices fabrication process**

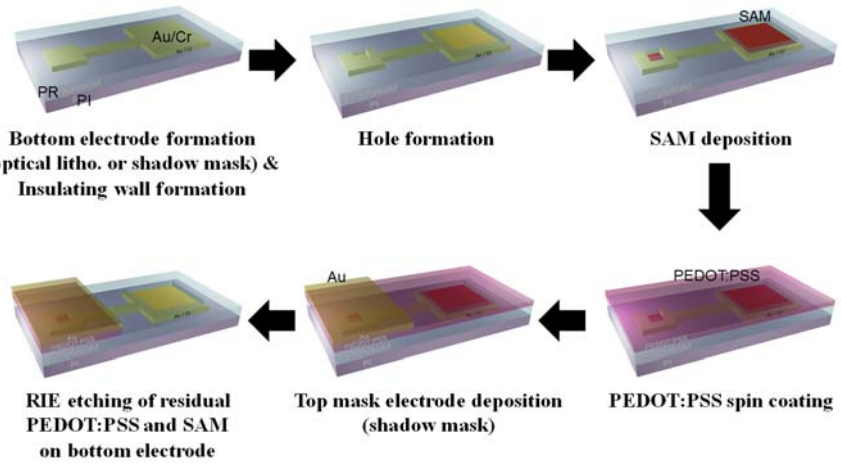


**Figure 2-3. Fabrication process of rectifying molecular devices on flexible substrates**

Figure 2-3 depicts a schematic of the fabrication procedure for ferrocene-alknaethiol composed of an alkanethiol with a terminal ferrocene moiety molecular devices on flexible substrate. First, Au (60 nm)/Ti (5 nm) was deposited on a polyimide (PI) substrate (Neopulim L-3430 purchased from Mitsubishi Gas Chemical Co., Inc.) using a shadow mask and electron-beam evaporator with a slow deposition rate of ~0.1 Å/s. Then, hexamethyldisilazane (HMDS) adhesion layer was spin-coated on the samples, followed by insulating photoresist (PR; Az5124E, purchased from Az Electronic Materials) that was spin-coated at 4,000 rpm for 1 min. Square-shaped holes with a side lengths ranging from 30 to 100 μm were made through the PR layer by conventional photolithography. The samples were hard-baked at 190 ºC for 3 hours. We choose three molecules in this experiment: 6-ferrocenyl-1-hexanethiol (FcC6), 8-ferrocenyl-1-octanethiol (FcC8), and 11-ferrocenyl-1-undecanethiol (FcC11). The molecules varied in length depending on the number of alkyl chains present ($(CH_2)_N$, where N = 6, 8, and 11; FcC6 and FcC11 are available from Sigma-Aldrich Co. and FcC8 is available from Dojindo Molecular Technologies, Inc.). For SAM deposition, we immersed the samples in this molecular solution for 1-2 days in an N2-filled glove box. After SAM deposition, the samples were washed by anhydrous ethanol to remove the residual molecules and then dried with $N_2$ stream in $N_2$-filled glove box for ~2 hour. The previously reported sandwich structure (metal-molecules-motel) junction are prone to electrical shorting due to the penetration of the top metal through the SAM during metal

evaporation, which makes conducting paths between the bottom and top electrodes [122-124]. To solve the electrical short problem in molecular junctions, a conducting polymer, PEDOT:PSS (poly(3,4-ethylene-dioxythiophene) with poly(4-styrenesulphonic acid); PH1000, from CLEVIOS) was spin-coated on the top of SAM before top electrodes was deposition on SAM [125]. Finally, top electrode Au (50 nm) was deposited on top of PEDOT:PSS with shadow mask, and redundant PEDOT:PSS was removed from the devices by a reactive ion etching (RIE) with oxygen.

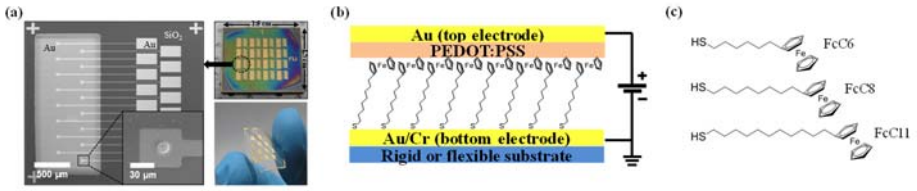


**Figure 2-4. Optical image on rigid and flexible substrates, SEM (b) Vertical structure type of molecular junction (c) 6-ferrocenyl-1-hexanethiol (FcC6), 8-ferrocenyl-1-octanethiol (FcC8) and 11-ferrocenyl-1-undecanethiol (FcC11)**

In this research, we have fabricated the ferrocene-alkanethiol molecular devices on both rigid and flexible substrates as shown in figure 2-4-(a). The rigid junctions were circular, with radii of 7, 8, and 9μm while the flexible junctions were squares with a side length from 30 to 100 μm with 10μm increment. The figure 2-4 consists of optical image of the molecular devices on both substrates, Scanning electron microscopy (SEM), schematic of the devices, and molecules structures.

# 2.2. Charge transport mechanism

To demonstrate that asymmetry value of ferrocene-alknaethiolate devices is consistent, we fabricate the ferrocene-alkaethiolate molecular devices on both rigid and flexible substrates, compared asymmetry value at two substrates. Figure 2-5-(a), (b) shows the representative asymmetrical current density–voltage (J–V) behavior of the three different length of ferrocene-alkanthiolate (FcC6, FcC8, FcC11) molecules on both rigid and flexible substrates. For convenience, the current density values of both substrates were plot absolute value at negative bias for comparison current density value of positive and negative bias. Alkyl molecules with ferrocene moieties have previously studied behavior of current level different between positive and negative bias, in which SAMs of these molecules were sandwiched between a Ag bottom electrode and a top electrode comprising eutectic Ga and In (EGaIn) [44, 48, 49]. In case of EGaIn top electrode, high rectification occurred because the highest occupied molecular orbital (HOMO) of the ferrocene moiety participated in charge transport under negative bias only. At a negative bias, the HOMO of ferrocene is located between the Fermi levels of the two electrodes and contributes to charge transport, whereas at a positive bias the HOMO of ferrocene is below the Fermi levels of both electrodes and therefore cannot contribute to charge transport [51]. We observed similar asymmetric electrical characteristics in our study but with somewhat lower asymmetric ratios. The asymmetric ratio (α), which is defined as $\alpha = | J(-1\ V)/J(1\ V) |$, where $J(\pm 1\ V)$ is the current density

measured at ±1 V, was lower (α = ~1.6) in this report. The observed low asymmetric ratio is due to the different junction structures employed, particularly for the top electrode material. And to ensure that the off unity asymmetric ratio is truly attributed to the ferrocene moiety, we could find from our previous reports that the estimated asymmetric ratio is clearly ~1 when the deposited molecules are lacking the ferrocene moiety but under same device configurations [147]. Therefore, the off unity asymmetric ratio evidently originates from the ferrocene moiety. To understand the origin of asymmetric electrical characteristics, Figure 2-5-(c) shows the energy band diagrams of our molecular junctions.

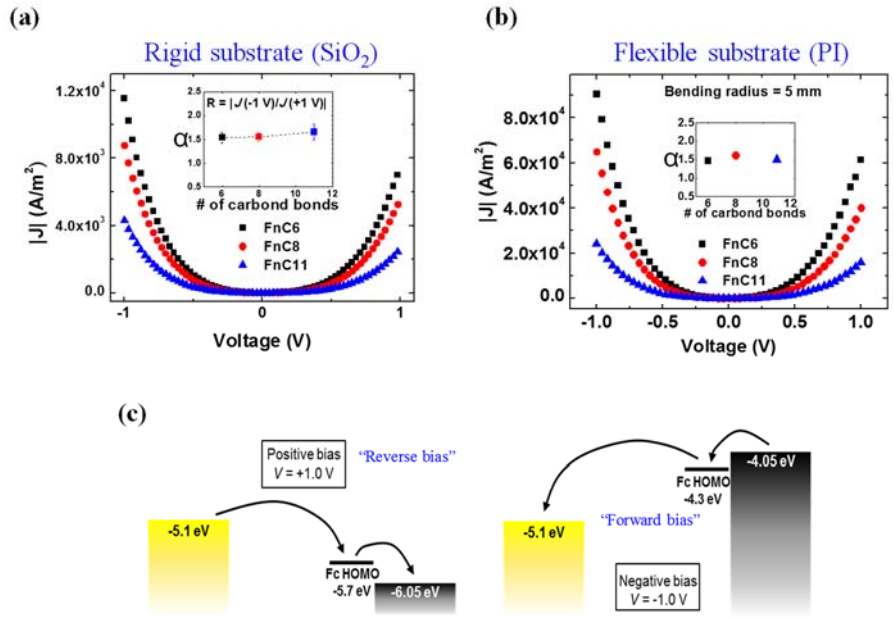


**Figure 2-5. (a), (b) J-V plots of rectifying molecular devices (c) Energy diagram of +1 V and -1 V**

The work function of Au is ~5.1 eV. The work function of PEDOT:PSS

was determined to be ~5.05 eV using a Kelvin probe measurement. The HOMO of the ferrocene moiety is ~ -5.0 eV (*i.e.*, 5.0 V below the vacuum level). The left and right schematics depict the energy band diagram when +1 V and -1 V are applied to the PEDOT:PSS side, respectively. Note that in this diagrams we assumed that there is potential drop of 0.3 V per applied 1 V due to van der Waals contacts between the ferrocene moiety and the PEDOT:PSS [44, 48-50]. Therefore, when +1 V is applied the HOMO of ferrocene decreases to -5.7 eV, whereas an applied bias of -1 V increases the HOMO to - 4.3 eV. To representative a high asymmetric ratio molecular devices, the HOMO of the ferrocene moiety should lie between the Fermi levels of the two electrodes under one bias polarity (forward bias) but lie below the Fermi levels of both electrodes at the other bias polarity (reverse bias). These locations enable a high asymmetric ratio because a HOMO that lies between the Fermi levels at the forward bias condition can act as a resonant energy state for charge transport [51]. However, in this report, the HOMO of ferrocene located between the Fermi levels of each electrode (PEDOT:PSS and Au) at both bias polarities. Thus, the HOMO of the ferrocene can participate in charge transport at both bias polarity conditions, resulting in the low asymmetric ratio (~1.6) observed in this report.

# 2.3. Redox process of ferrocene-alkanethiol molecules

We suggest that one possible model of the reason of exhibit and small asymmetry value can be conformational change of ferrocene-alkanethiol and disordering of ferrocene moiety part due to redox process.

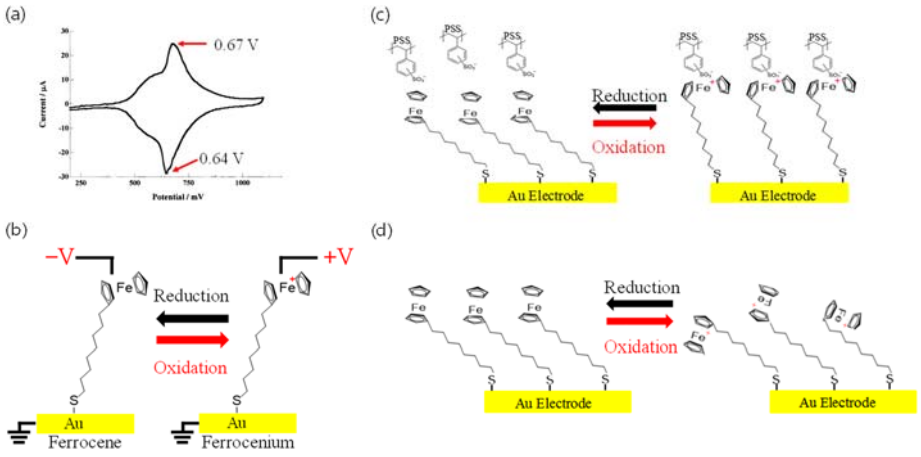


**Figure 2-6. (a) Cyclic voltammogram of rectifying molecules (b) Oxidation and reduction process of ferrocene-alknaethiol (c) More standing up configuration of the alkyl chain part (d) Disordering of ferrocene moiety**

In figure 2-6-(a), cyclic voltammogram(CV) show oxidation and reduction of ferrocene-alkanethiol molecules on gold electrode, in previous report [166, 167]. Oxidation and reduction peak of ferrocene moiety was recorded at +0.67 and 0.64 V, respectively. In this process, because ferrocene terminal group is very strong electron-donating, ferrocen change to ferrocenium cation, as shown figure 2-6-(b). When ferrocene moiety oxidize to ferrocenium cation with high than ~0.6 V, ferrocenium interact $SO_3^-$ part of PSS with attractive force while oxidized ferrocene end group react positively charge gold electrode with

repulsive force. The attractive interaction between ferrocenium cation and $SO_3^-$ part of PSS and the repulsive interaction between positive $Fc^{+2}$ and positively charged Au surface can be the conformational change of ferrocene-alkanethiolate, resulting of more standing up molecular layer, like figure 2-6-(c). In addition, oxidized ferrocene happen disordering because ferrocenium cation exert electrostatic repulsion randomly at neighbourhood oxidized ferrocene end group as shown figure 2-6-(d). Disordering of ferrocenium cation cause the instability contact between ferrocene moiety and PEDOT:PSS. As results, the current density of the molecular devices reduced at only positive bias [147, 168].

# 2.4. Mechanical deformation of molecular devices

To test electrical characterization of the molecular devices under mechanical deformation, we measured the current density of FcC6, FcC8, FcC11 under physical strain with severe different bending radii and a large repetitive number of bending cycles (defined form flat(∞) to bent 5 mm as shown figure 2-7-(b) inset).

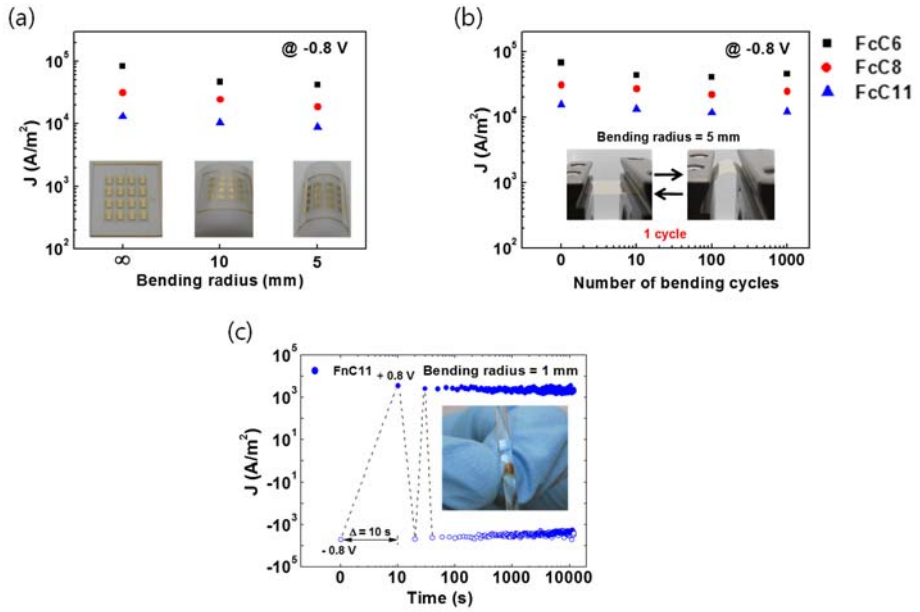


**Figure 2-7. J-V plot of FcC6, FcC8, FcC11 molecular devices under the same banding conditions (a) Bending radii (flat, 10 mm, 5 mm) (b) Bending cycles (10, 100, 1000 times, bending radius = 5 mm) (c) J value at alternative -0.8 V and +0.8 V of FcC11 molecular device wound at 1 mm cylindrical**

Under the mechanical deformation, three difference of length ferrocene-alkanethiolate devices maintain own electrical properties (i.e. current density with comparison flat conditions, asymmetry value ~1.6). To test devices performance under extremely bending condition, we wound up the FcC11 device at a cylindrical bar with bending radius of 1 mm. When the retention properties of the device in this bending condition were investigated, it was found that the current density of FcC11 devices was consistent for up to $10^4$ seconds with asymmetry value. In this plots, we demonstrated that the electrical characteristics of rectifying molecular devices do not suffer any significant deterioration during mechanical stressing, and the current density was similar

to that measured for the flat substrate condition(previous J-V plot) with asymmetry value regardless of the bending radius configuration.

All these results demonstrated that the flexible molecular-scale devices containing photoswitching diarylethene molecules were reliably fabricated and operated with excellent stability when subjected to various mechanical stresses.

# 2.5. Conclusion

In summary, we studied the redox-induced electronic transport properties of ferrocene-alkanethiolate molecules using a conducting polymer-interlayer device structure both of rigid and flexible substrates. We observed asymmetric electrical transport characterization both of two kind substrates, which arise due to the existence of ferrocene moiety. Because of redox process of ferrocene moiety at ~ +0.6 V, oxidized ferrocene can be conformational change of the SAM and happen disordering neighborhood ferrocnenium cation each other. As result, these phenomena of ferrocene moiety show asymmetry behavior of the molecular devices. We also demonstrated asymmetric current density-voltage performance under various bending configurations. The ferrocene-alknaethilate molecular devices on flexible do not show seriously current level change and maintain asymmetric behavior under server bending conditions.

# Chapter 3 Photoswitching molecular devices with PEDOT:PSS/Au top electrode

## 3.1 Introduction

In the chemistry, isomerization is the molecules characteristic by which one molecules has two independent states by reaction from outside specific conditions like light, thermal, voltage, additive etc. There are several kinds of isomerization phenomena; Linkage Isomer, Isomerization of Hydrocarbon cracking, Aldoes-Ketose Isomerism, Cycloisomerization, Photoisomerization.

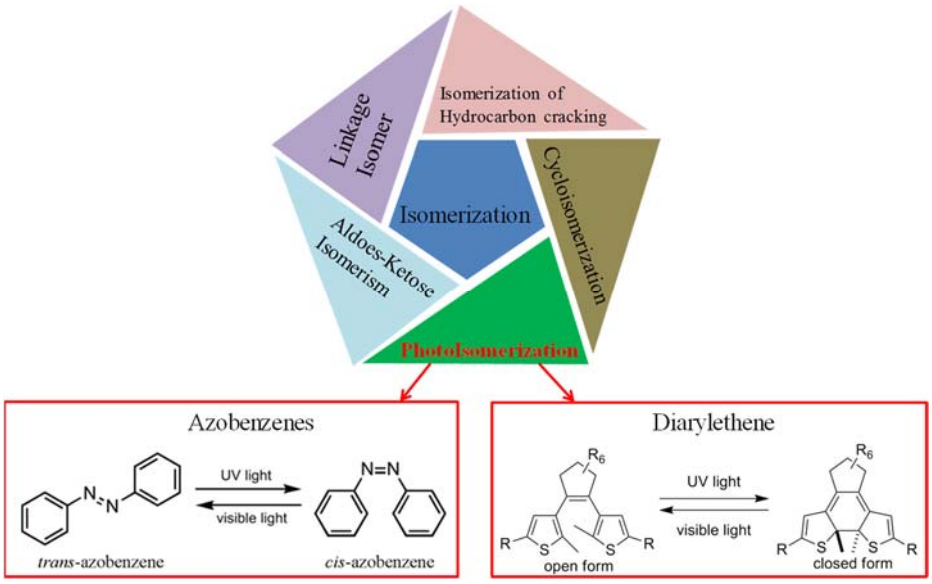


**Figure 3-1. Isomerization types: Photosiomerization type molecules(Azobenzens, Diarylethene)**

In those, photoisomerzation is defined as one molecule reacts with light of certain wavelength band and has two electrical states of high conductivity state and low conductivity state. The most studied photoswitching molecules are azobenzene and diarylethene. Azobenzene reacts with U.V light, changes from trans to cis form, reacts with visible light, and change cis into trans. This is a phenomenon in which the molecule itself is physically bent. Diarylethene is a chemical modification of combination or termination of molecular orbital and reacts with U.V light, changes from open to closed form, reacts with visible light, and change closed form into open form.

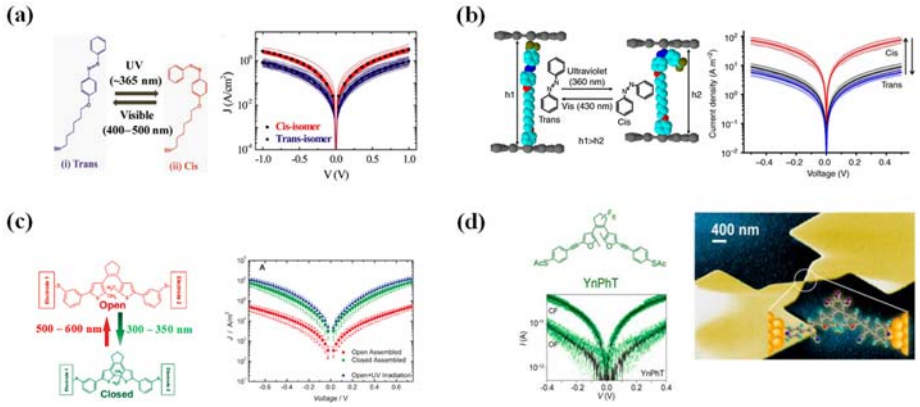


**Figure 3-2. (a) Azobenzen derivative structure and J-V plot of two states (b) Azobenzen molecular devices on graphene and switching phenomena (c) Diarylethene chemical structure and J-V plot of two states (d) Single diarylethene molecular device**

Figure 3-2-(a), (b) show electrical characterization of azobenzen linked to alknaethiol deposited Au and graphene layer bottom electrode [66, 67]. The main mechanism of both cis and trans is tunneling through temperature variable current density – voltage [73, 130]. When compared the molecular length of both states (i.e. trans ~22 Å, cis ~19 Å), the conductance of cis states is expected to be higher than trans and the results were also the same, as shown the two figure above. In addition, the azobenzen derivative deposited on graphene layer shows successful isomerization phenomenon which switches reversibly from trans to cis with illumination UV or from cis to trans with visible light [73]. In case of diarylethene, the open ring change to closed form with UV light irradiation leading to a completely π-conjugated system, while the closed ring change to open form with visible light, breaking up molecular system. The π-conjugated system of closed form is supposed to lead to higher conductance than broken one. As shown figure 3-2-(c) and (d), the conductance of closed

form higher than open form in the case of SAM layer [58] and single molecule [72].

- **Devices fabrication process**

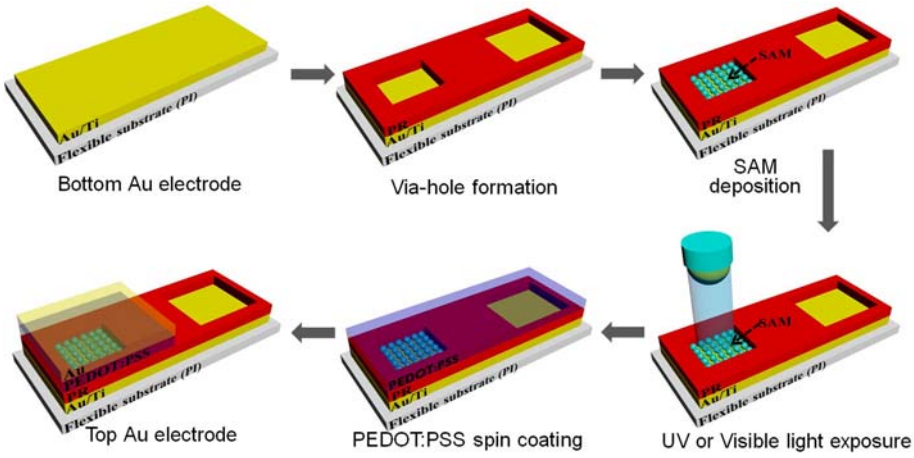


**Figure 3-3. Fabrication of photoswitching molecular devices on flexible substrates**

Figure 3-3 illustrates the device fabrication processes for diarylethene species molecular electronic devices on a flexible substrate. First, Au (60 nm)/Ti (5 nm) was deposited on a polyimide (PI) substrate (Neopulim L-3430 purchased from Mitsubishi Gas Chemical Co., Inc.) using a shadow mask and electron-beam evaporator with a slow deposition rate of ~0.1 Å/s. Then, hexamethyldisilazane (HMDS) adhesion layer was spin-coated on the samples, followed by insulating photoresist (PR; Az5124E, purchased from Az Electronic Materials) that was spin-coated at 4,000 rpm for 1 min. Square-shaped holes with a side lengths ranging from 30 to 100 μm were made through the PR layer by conventional photolithography. The samples were hard-baked at 190 $^{o}$C for 3 hours. For deposition of the self-assembled monolayer (SAM)

diarylethene molecules on the exposed Au bottom electrode's surface, we prepared a diluted solution of diarylethene molecules (~ 3 mM) in ethanol and added a small amount of ammonium hydroxide ($NH_4OH$) to the molecular solution to de-protect the acetyl ($COCH_3$, denoted as Ac) group from the thiol end-group for enabling electrical contract to the bottom gold electrode [72]. Then, we immersed the samples in this molecular solution for 1-2 days in an N2-filled glove box. After SAM deposition, the samples were washed by anhydrous ethanol to remove the residual molecules and then dried with $N_2$ stream in $N_2$-filled glove box for ~2 hour. Then, the samples were exposed to UV handed lamp capable of generating 312 nm UV light or visible light lamp (fluorescent lamp) in a dark room for ~1 hour to determine the open or closed state of diarylethene molecules. To minimize the electrical short problem in the molecular junctions, a conducting polymer, PEDOT:PSS (poly(3,4-ethylene-dioxythiophene) with poly(4-styrenesulphonic acid); PH1000, from CLEVIOS) was spin-coated on the top of SAM [125]. Finally, top electrode Au (20 nm) was deposited on top of PEDOT:PSS with shadow mask, and redundant PEDOT:PSS was removed from the devices by a reactive ion etching (RIE) with oxygen.

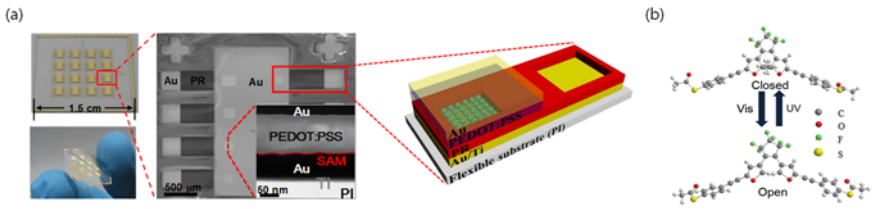


**Figure 3-4. (a) Optical image, SEM, TEM and illustration of photoswitching molecular devices on flexible substrates (b) Chemical structure of diarylethene**

This figure 3-4 shows a series of optical, scanning electron microscopy (SEM), and cross-sectional transmission electron microscope (TEM) images of the fabricated molecular devices on the flexible substrates. The photoswitching molecules can convert from open and closed state with irradiation of UV or from closed and open with illumination of visible light as shown molecular structure figure.

# 3.2 Electrical characteristics, stability, reliability

Figure 3-5-(a) shows the current density-voltage (J-V) data from the diarylethene molecular devices in the open and closed states under a flat substrate condition (defined as having a bending radius = ∞). We determined that the current observed in the closed state was higher than that from the open state by an order of magnitude, as has been found earlier for similar devices from thiophene-based diarylethenes on Si-based rigid substrates [58]. The high

current density (~$10^6$ A/m$^2$ at 0.8 V) observed in our devices reflects the SAM formation with our novel high-yield, flexible-substrate process.

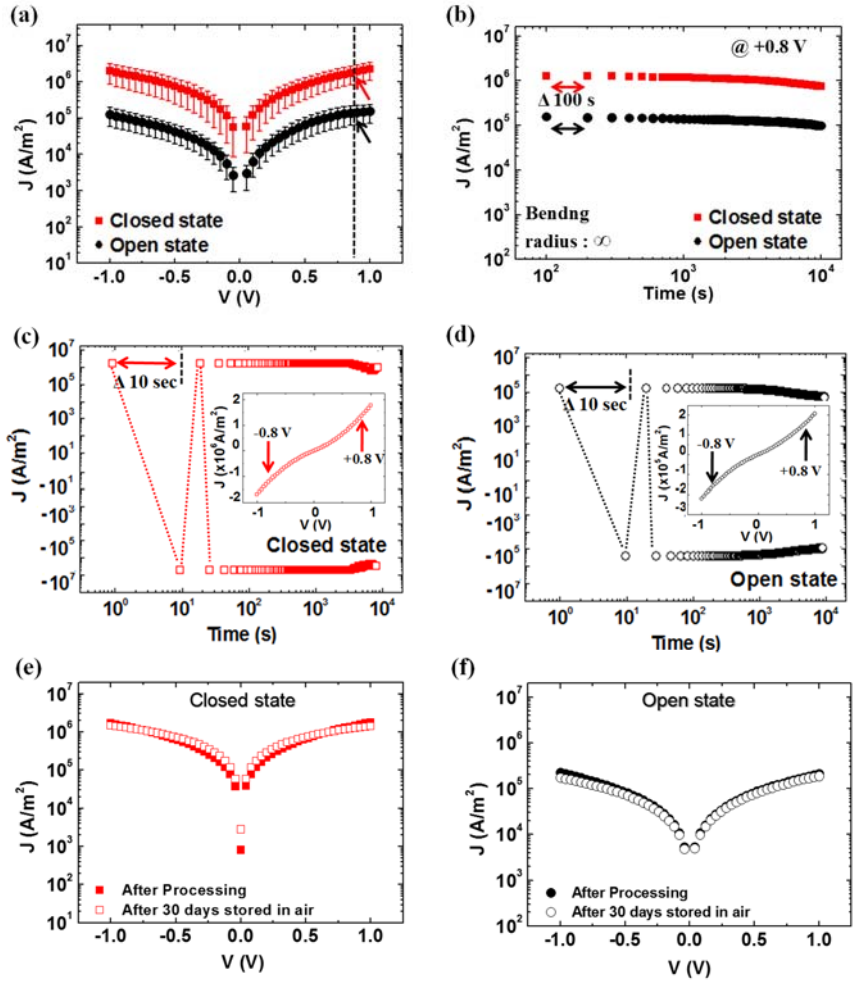


**Figure 3-5. J-V plots of the closed and open states (b) Retention characteristics for the closed and open states (c), (d) Endurance characteristics of the closed and open states (e), (f) Comparison of J values of the closed and open states with after processing, after 30 days stored in air**

The electrical conductance discrepancy has been understood to arise from the pi-conjugated system of closed state and broken pi-conjugated system of open state. The open state changes to the closed states by forming a completely

pi-conjugated system with illumination UV light. Conversely, closed state changes to the open states with broken pi-conjugated system when exposed to visible light. As a result, the energy gap between the highest occupied molecular orbital (HOMO) and the lowest unoccupied molecular orbital (LUMO) of the closed state is smaller than that of the open state. In addition, the broadening of HOMO-LUMO level related electrical conductance of photoswitching molecular devices is defined by Gamma(Γ) value which is coupling constant. Because the Gamma value of closed state is bigger than open ones, the metal-molecule contact (Au-thiol) of the closed state was found to give rise to a stronger broadening of the current-carrying molecular orbital than that of the open state, which also signals the stronger conjugation in the closed state [72]. Lastly, the molecular length of open states is longer than closed through molecular dynamic simulation. The length different between two states induce that tunneling length increase at open state. As a net result, the current of the closed state is higher than that of the open state.

Additionally, we investigated the retention properties, i.e., the stability of the electrical characteristics of the photoswitching molecular devices on flexible substrate with open and closed state under a flat substrate condition by measuring the current density at 0.8 V over a long period, as shown in Figure 3-5-(b). Specifically, the current density was measured in the open and closed states for up to $10^4$ seconds at an increment of 100 seconds. The current density of each state and the discrepancy between the two states were well maintained.

This result indicates that both of the molecular device states (open and closed states) did not degrade when subjected to repeated voltage stresses.

We also investigated the endurance stability of the open and closed states by measuring the current density at alternating voltages of ±0.8 V for up to $10^4$ seconds at an increment of 10 seconds. Figures 3-5-(c) and (d) show the current density results on a logarithmic scale for the closed and open states, respectively. The insets of Figures 3-5-(c) and (d) show the J-V curves before the endurance test for the closed and open states, respectively. The current density was observed to be almost constant without any significant degradation. We also measured the J-V curves of the open and closed states after the devices were stored for 30 days under ambient conditions, as shown Figure 3-5-(e) and (f). In these measurements, we did not observe any noticeable degradation and well maintain the discrepancy between the two states. All these results indicate that the devices retain their electrical properties well, demonstrating the stability and reliability of diarylethene molecular devices in both photoswitching states.

➢ **Electrical characterization of the photoswitching molecular devices under bent conditions**

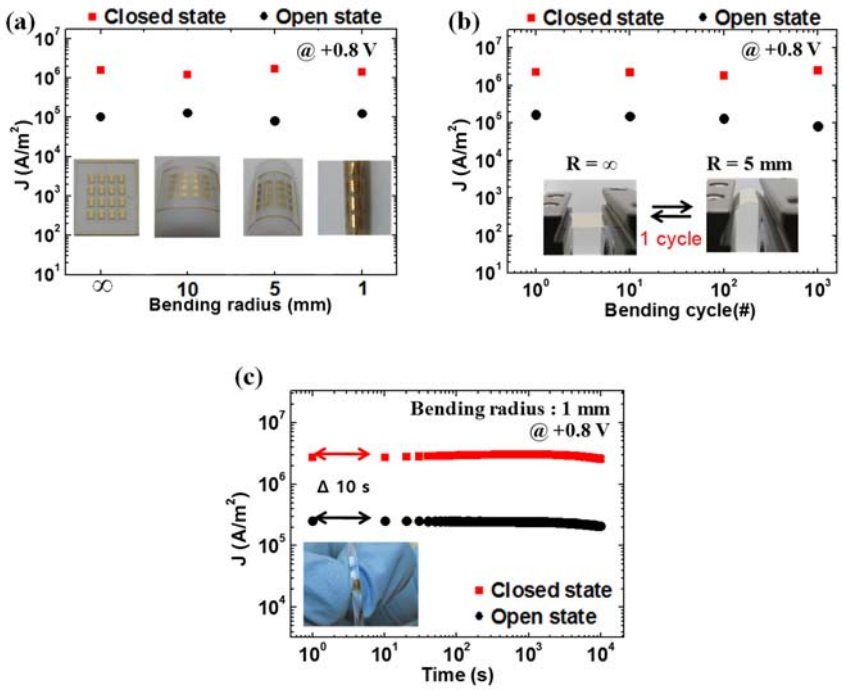


**Figure 3-6. J-V plot of the closed and open states photoswitching molecular devices under the same banding conditions (a) Bending cycles (10, 100, 1000 times, bending radius = 5 mm) (b), Bending radii (flat, 10 m, 5 mm) (c) Retention characteristics of the closed and open states wound up at 1 mm cylindrical bar**

To further test the robustness of these devices in view of applications making use of the flexibility of the device, we examined the electrical characteristics of the open and closed states when the device is subjected to mechanical deformation with severe different bending radii and a large repetitive number of bending cycles (defined form flat(∞) to bent 5 mm as shown figure 3-6-(a) inset). Figure 3-6-(b) displays the current densities for the two states measured at 0.8 V under various bending configurations (bending

radii equal to ∞ (flat), 10 mm, 5 mm, and 1 mm). The currents from the two states were also measured while being subjected to up to $10^3$ bending cycles, as shown in Figure 3-6-(a). To investigate under extremely bending condition, we wound up the photoswitching molecular devices at a cylindrical bar with bending radius of 1 mm. When the retention properties of the device in this bending condition were investigated, it was found that the currents for the open and closed states were consistent for up to $10^4$ seconds with an order of magnitude difference between the two states. In this plots, we demonstrated that the electrical characteristics of both the open and closed states do not suffer any significant deterioration during mechanical stressing, and the current density was similar to that measured for the flat substrate conditions(previous J-V plot) with an order of magnitude difference between the two states regardless of the bending radius configuration.

All these results demonstrated that the flexible molecular-scale devices containing photoswitching diarylethene molecules were reliably fabricated and operated with excellent stability when subjected to various mechanical stresses.

# 3.3 Temperature-variable current-density voltage

To investigate the charge conduction mechanisms of the open and closed states, we measured temperature-variable current density-voltage (J-V-T) measurements under flat and bent substrate conditions

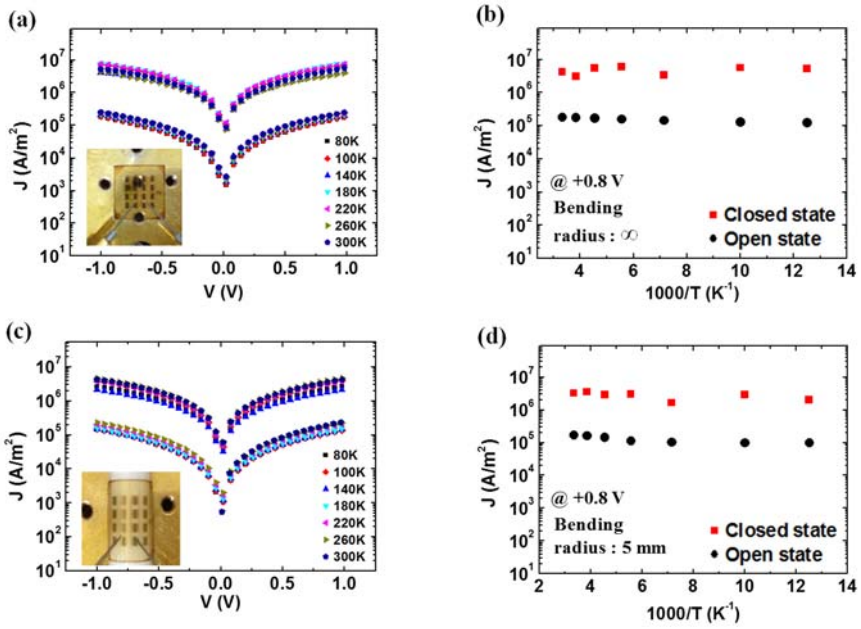


**Figure 3-7. Temperature-variable J-V plots, Arrhenius plots of the closed and open states under flat (a), (b) and 5 mm bent condition (c), (d)**

Figure 3-7-(a) and (c) show the J-V-T results for the two states for a flat condition and mechanical deformation condition with bending radius of 5 mm at variable temperatures from 80 to 300 K with 20K increment. Figure 3-7-(b) and (d) show the Arrhenius plots (i.e., the current density versus the inverse of the temperature) of two states under flat and bending condition (r=5 mm)

created from the data shown in Figure 3-7-(a) and (c). We observed that the current density for both states did not change noticeably when the temperatures varied under both the flat and bent substrate conditions (Figure 3-5). These results suggest that the main electrical conduction mechanism for the diarylethene molecules is tunneling for both the open and closed states, regardless of any mechanical deformation.

# 3.4. Conclusion

In summary, we have fabricated molecular-scale electronic devices with photoswitching diarylethene molecules on flexible substrates. The diarylethene molecular devices exhibited either high (Closed state) or low (Open state) electrical conductance states when exposed to UV or visible light during fabrication, respectively. The conductance in both states are sufficiently high to be measured and differ by an order of magnitude making them easy to discriminate with standard electronics. The electrical properties of the diarylethene molecular devices were found to be constant under variable temperature, repeated voltage cycling, various mechanical deformation configurations, including varying the bending radius (down to 1 mm) and subjecting the substrates to repeated bending cycles, demonstrating that the molecular state as well as the contact geometry are robust. The current flowing in each state is dominated by a tunneling conduction mechanism regardless of any mechanical deformation.

# Chapter 4

# Photoswitching molecular devices with reduced graphene oxide top electrode

## 4.1. Introduction

Because the PEDOT:PSS/Au top electrode with low transmittance prevent UV or visible light from penetrating phoswitching molecular layer, the properties of isomerization with reversible change phenomena as basic concept may not be shown [130]. To solve this problem and represent isomerization properties, a new attempt is to convert existing top electrode into graphene high transmittance and conductivity. Not only this, but two-terminal molecular devices on graphene have advantage of chemically stable, transmittance, conductivity and mechanically flexible. Especially, azobenzen derivative based

on graphene devices have been successfully represented of cis and trans electrical characterization, addition to isomerization properties.

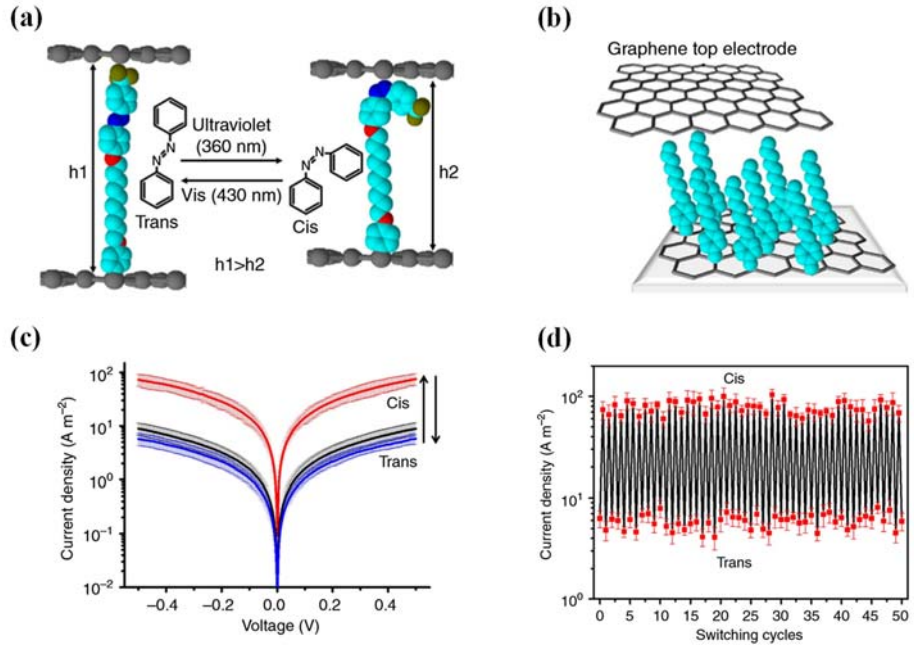


**Figure 4-1. (a), (b) Schematic of azobenzene derivative molecule devices on graphene layer (c) The J-V plots of cis and trans states (d) reversible switching phenomena**

Figure 4-1-(a), (b) show to azobenzen photoswitching molecular devices on graphene layer. This molecules changes from trans to cis from with UV irradiation, while it changes from cis to trans with illumination visible light. As a such physical deformation, the azobenzen molecules of cis and trans forms of length itself is changed, so that the tunneling length is different ($h_1 > h_2$). Because the main mechanism of azobenze derivative is tunneling effect, the conductance of cis form is better than trans one, as shown figure 4-1-(c). Importantly, reversible photoswitching phenomena appeared repeatedly more than 50 times at the molecular devices like figure 4-1-(d). The photoswitching

molecular devices based on graphene with high transmittance showed perfectly isomerization properties which is reversible switching between two states. If the top electrode of diarylethene devices is changed from PEDOT:PSS/Au top electrode to graphene, the switching characterization will happen surely.

## ➢ Devices fabrication process

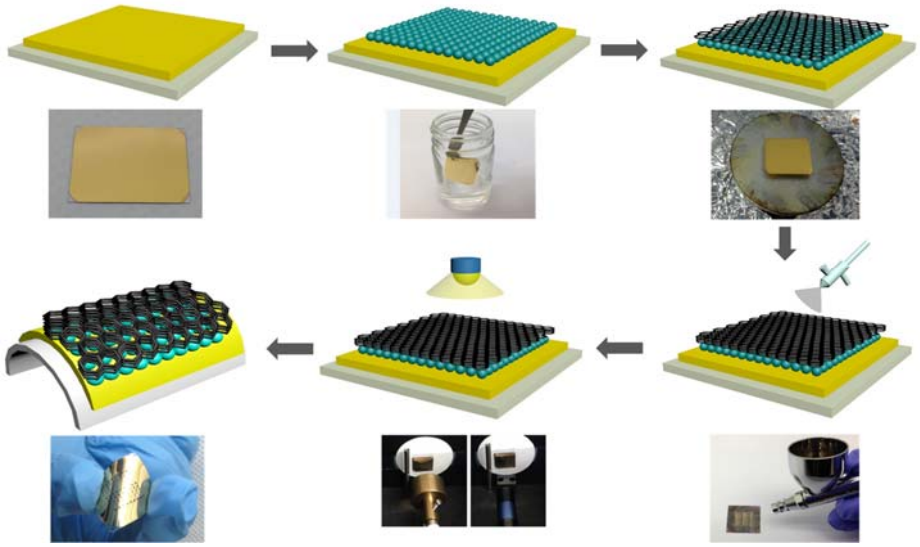

**Figure 4-2. Fabrication of diarylethene photoswitching molecular devices on flexible substrates with reduced graphene oxide(rGO)**

Figure 4-2 shows the schematics illustrating the fabrication processes. After cleaning the plastic flexible substrates with isopropyl (IPA) and distilled (DI) water, the bottom electrode Au (60 nm)/Ti (5 nm) was deposited on a poyethylene terephthalate (PET) flexible substrate (purchased from Sigma-Aldrich Korea Ltd.,) by using an electron-beam evaporator at a slow deposition rate of ~0.1 Å/s to obtain a smooth surface for the bottom gold electrodes. For deposition of the self-assembled monolayer (SAM) photoswitching molecules

on Au bottom electrode's surface, we prepared a diluted solution of diarylethene molecules (~3 mM) in ethanol and added a small amount of ammonium hydroxide ($NH_4OH$) to the molecular solutions to de-protect the thiol group of the diarylethene molecules, so that the thiol end-group enables good electrical contact to the bottom gold electrodes by thiol-Au chemisorption [72]. Next, the samples were immersed in this molecular solution for 1-2 days in an $N_2$-filled glove box. After SAM deposition, reduced graphene oxide (rGO) in dimethylformamide (DMF) was spin-coated twice over the SAMs to protect from any outside contaminants. During the photoswitching molecular devices fabrication, the samples were exposed to a UV (360 nm) laser for ~1 h or a visible (520 nm) laser for ~ 30 min to be defined as the closed state or open state, respectively. Finally, the rGO top electrode was made by spraying rGO solutions through a shadow mask with a side length from 200 to 600 µm.

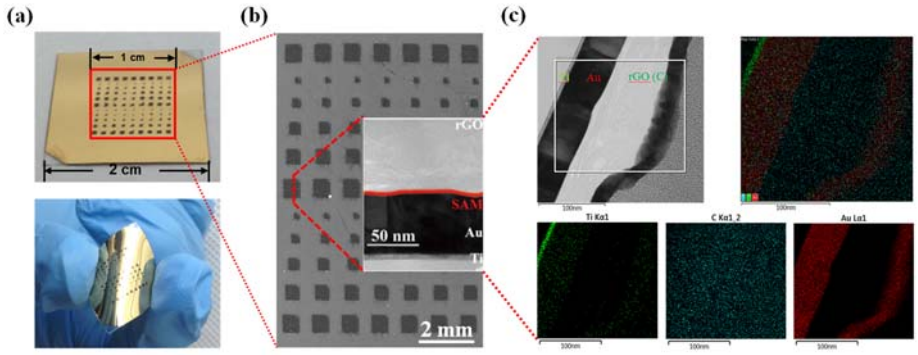


**Figure 4-3. (a) Optical, (b) SEM and (c) TEM images of photoswitching molecular devices**

Figure 4-3 shows a series of optical images and scanning electron microscopy (SEM) and transmission electron microscopy (TEM) images of the fabricated photoswitching molecular devices with rGO top electrode on flexible

substrate. In the TEM images, each layer (Ti, Au and C) were well formed through mapping method.

## 4.2. Electrical characterization of rGO top electrode

To demonstrate that reduced graphene oxide can be used as good transparent and conducting electrodes photoswitching molecular devices on a plastic substrates, we measured the transmittance, current-voltage graph, Raman spectra, and X-ray photoelectron spectroscopy (XPS) data for an rGO film. Figure 4-4-(a) shows transmittance plots for an rGO film and a PEDOT:PSS/Au film. Previously, we used a PEDOT:PSS/Au film as the top electrode for photoswitching molecular devices, but those devices failed to show the reversible photoswitching phenomenon [68]. The absence of reversible photoswitching in the molecular devices with PEDOT:PSS/Au top electrodes could be caused by the relatively low transmission characteristics of PEDOT:PSS/Au compared to those for an rGO film.

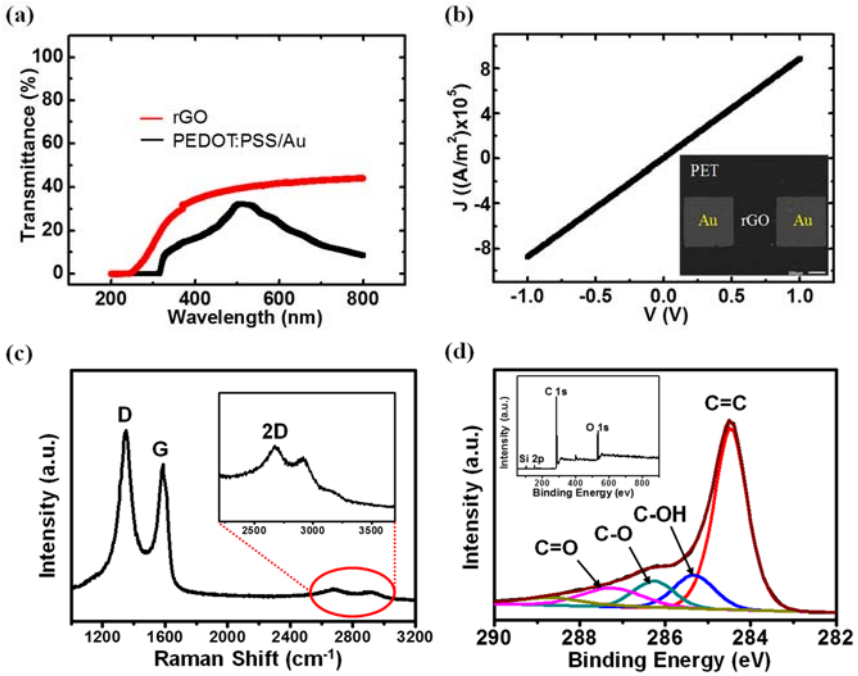


**Figure 4-4. (a) Transmittance rGO and PEDOT:PSS/Au (b) Conductivity of rGO (c) Raman spectroscopy (d) X-ray photoelectron spectroscopy**

We also checked the conductivity of the rGO film. For this, we fabricated a pattern with an rGO film in contact with two Au electrodes (see inset of Figure 4-4-(b)) and measured the current density-voltage (J-V) characteristics. From this J-V plot, we found the conductivity of an rGO film to be 3700 S/m [169]. The results of Figures 4-4-(a) and (b) indicate that an rGO film can be used as the top electrode in photoswitching devices. We observed the typical G, D, and 2D peaks that were located at 1590, 1350, and 2910 $cm^{-1}$, respectively. It is well known that G-mode is a primary in-plane vibrational mode, indicating C-C $sp^3$ stretching. The D-mode is a first or second order overtone for a different in-plane vibration, indicating a structural defect in the crystal where C=C $sp^2$ is

created because of C-C $sp^3$ bond formation [170, 171]. The XPS data of rGO are shown in Figure 4-4-(d). The XPS peak at 284.5 eV (C 1s peak) is assigned to the carbon atoms in C=C bond. XPS peaks at 285.3, 286.3, and 287.3 eV correspond to C-OH, C-O, and C=O, respectively [172, 173]. The XPS results indicate that graphene oxide was reduced enough to be used as top electrode.

# 4.3. Electrical characterization of photoswitching molecular devices with rGO top electrode

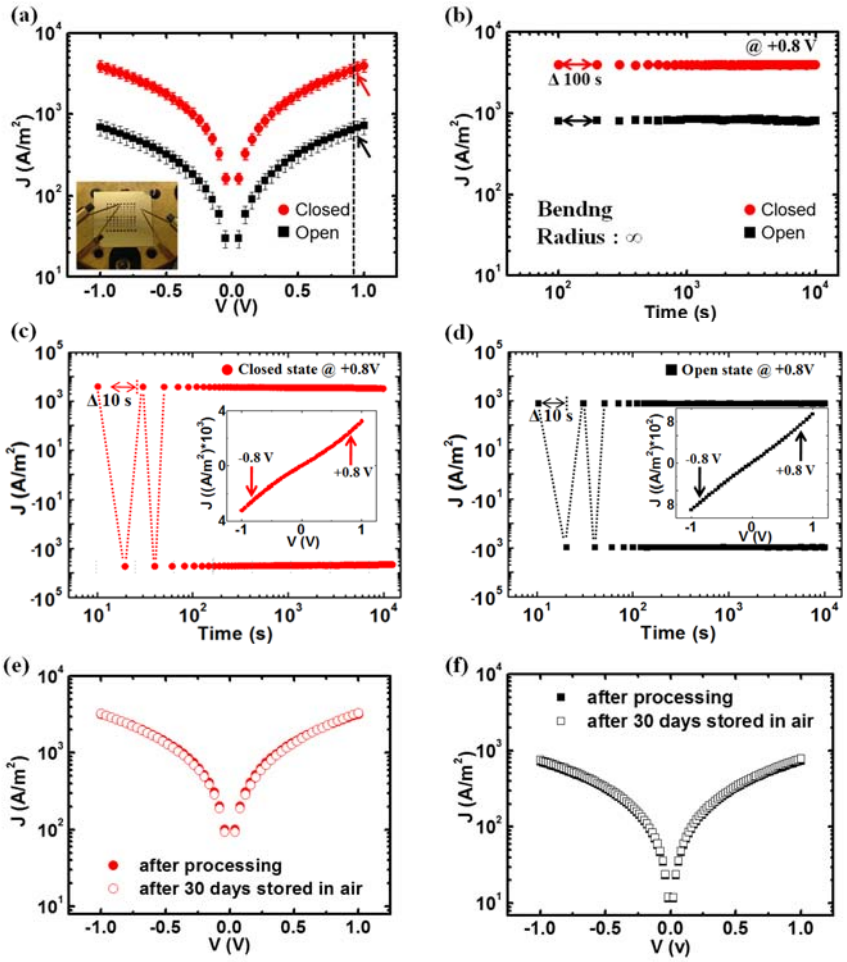


**Figure 4-5. J-V plots of the closed and open states (b) Retention characteristics for the closed and open states (c), (d) Endurance characteristics of the closed and open states (e), (f) Comparison of J values of the closed and open states with after processing, after 30 days stored in air**

Figure 4-5-(a) shows the J-V data from the diarylethene molecular devices

on flexible substrates with reduced graphene oxide(rGO) top electrodes in the open and closed states under a flat substrate condition (having a bending radius = ∞). The open and closed states were defined and fixed during device fabrication to exposure UV or visible laser. We confirmed that the current of the closed state was higher than that of the open state, as has been observed for the molecular junctions with PEDOT:PSS/Au top electrode [58]. There are three mechanisms resulting in the different electrical currents of the closed and open states [73]. Firstly, when the open state is exposed to UV light, the open state changes to the closed state by forming a completely π-conjugated system (see Figure 4-5). Equivalently, when the closed state is exposed to visible light, the closed state changes to the open state and the π-conjugation is broken (see Figure 4-5). As a result, the energy gap between the highest occupied molecular orbital (HOMO) and the lowest unoccupied molecular orbital (LUMO) of the closed state is smaller than that of the open state. Second, in the transport experiments of similar diarylethene molecules, the level broadening defined coupling constant (Gamma: Γ) of the current carrying molecular orbital of the closed state was found to be bigger than that in the open state, although the level alignment between the current-carrying molecular orbital and the Fermi energy of the Au electrodes was found to be better in the open state than in the closed state. Lastly, the molecular length of open states is longer than closed through molecular dynamic simulation. The length different between two states induce that tunneling length increase at open state. As a net result, the current

of the closed state is higher than that of the open state [72].

To investigate the stability and reliability of our photoswitching molecular devices with an rGO top electrode, we measured the current density (J) at +0.8 V for the closed and open state under flat (as defined r = ∞) conditions for up to $10^4$ seconds in increments of 100 seconds (Figure 4-5-(b)). Additionally, we measured the J values for alternating voltages of ±0.8 V under flat conditions for up to $10^4$ seconds with an increment of 10 seconds (Figures 4-5-(c) and (d)). The graphs of Figure indicate that photoswitching molecular devices with an rGO top electrode do not show any noticeable degradation during the retention measurements for the two electrical states. Moreover, we measured the J values of the closed and open states after the devices were stored for 30 days under ambient conditions, as shown Figure 4-5-(e) and (f). We did not observe any serious degradation of the devices in this test. Compared with the photoswitching molecular devices with PEDOT:PSS/Au top electrode, all of these results indicate that the devices with an rGO top electrode also is proved stability and reliability, maintaining good electrical properties for a long period of time.

# 4.4. Electrical characterization of photoswitching molecular devices under mechanical deformation

To test the photoswitching molecular devices with an rGO top electrode under mechanical deformation, we measured the J values of the closed and open states under several bending conditions.

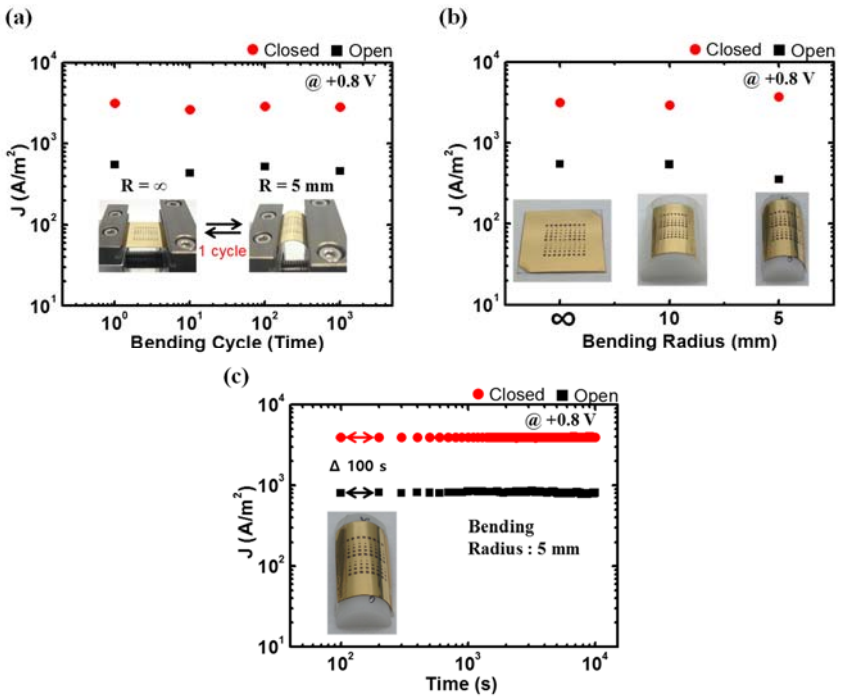


**Figure 4-6. J-V plot of the closed and open states photoswitching molecular devices under the same banding conditions (a) Bending radii (flat, 10 mm, 5 mm) (b) Bending cycles (10, 100, 1000 times, bending radius = 5 mm) (c) Retention characteristics of the closed and open states under 5 mm bent**

Figures 4-6-(a) and (b) show the J values at +0.8 V for the closed and open states under bending cycles (0, 10, 100, and 1000 times) and bending radii (∞,

10, and 5 mm). Additionally, we measured the J values for the closed and open states for up to $10^4$ seconds under a 5 mm-bending radius condition (Figure 4-6-(c)), indicating that the photoswitching molecular devices with an rGO top electrode maintained consistent J values with different current levels for each state during the retention measurements. The results presented in Figure 4-6 demonstrate that our devices on the flexible substrates were operated reliably and with good stability under the various bending conditions.

# 4.5. Reversible switching phenomenon of photoswitching molecular devices

To demonstrate continuative switching properties of the photoswitching molecular devices with rGO top electrode, we examined the reversible photoswitching phenomenon in our molecular devices. The photoswitching devices should reversibly switch between the two electrical states in response to the light illumination.

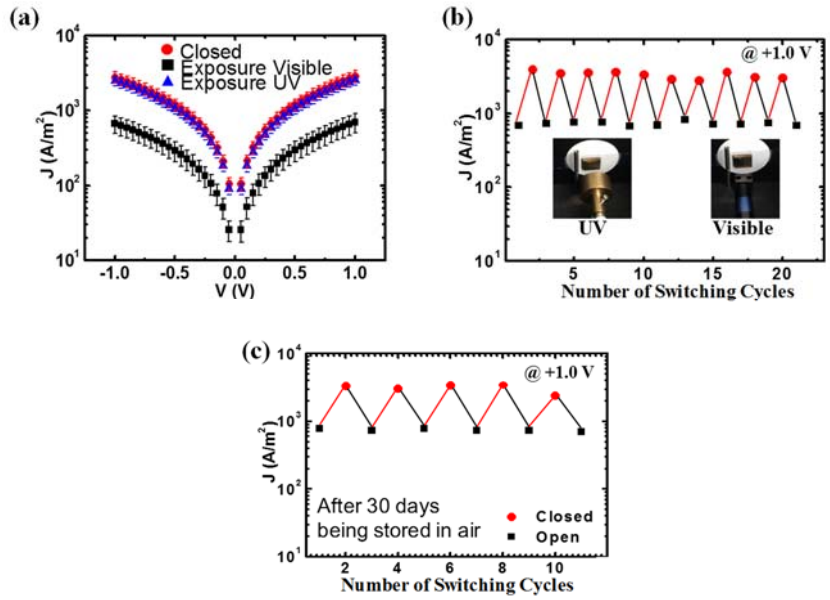


**Figure 4-7. (a) J-V curves of the photoswitching molecular devices at initial closed states (red circles), open states that were converted from the closed states with visible light illumination (black rectangles), and closed states that were converted from the open states with UV illumination (blue triangles). (b) The reversible photoswitching phenomenon repeated 20 times by alternating UV and visible light irradiation (c) The reversible photoswitching phenomenon after 30 days being stored in air**

Figure 4-7-(a) shows the J-V plots for the initial closed states (red circles), J-V plots for conversion to the open states after exposure to visible light (black rectangles, from the closed to open state), and J-V plots for conversion to the closed states after exposure to UV (blue triangles, from the open to closed state). The current levels of the photoswitchable open and closed states were consistent when compared to the data in (previous Figure 4-7-). We measured the reversible photoswitching phenomenon 20 times by alternating between irradiation with a UV and a visible laser; the results are shown in Figure 4-7-(b). In addition, we measured the reversible photoswitching phenomenon after

the devices were stored for 30 days in ambient conditions in figure 4-7-(c). With these results, we were able to prove that the diarylethene molecular devices with an rGO top electrode exhibited a reliable and reversible photoswitching phenomenon in response to illumination.

# 4.6. Conclusion

In summary, we have fabricated photoswitching molecular devices of the photoswitching molecular devices with reduced graphene oxide (rGO) top electrode on a polyethylene terephthalate (PET) flexible substrate. The photoswitching molecules (diarylethene) have two electrical conductance states: a high (Closed) conductance and a low (Open) conductance state, established by UV or Visible light irradiation. Unlike the molecular devices with PEDOT:PSS/Au top electrodes that failed to show the reversible photoswitching phenomenon because of low power handed UV or visible lamp, low transmittance of PEDOT:PSS/Au top electrode and vertical structure of the devices, we successfully demonstrated the reliable and reversible photoswitching phenomenon in molecular devices with rGO top electrodes upon exposure to UV or visible light. Additionally, the electrical properties of our photoswitching molecular devices with an rGO top electrode were well maintained under various mechanical deformations.

# Chapter 5

# Summary

In this thesis, we fabricated the rectifying, photoswitching molecular devices on flexible substrates and studied electrical characterization of the molecular devices under mechanical deformations which are several bending radii and a large number of repeated bending cycles. In addition, we analyzed the main charge transport mechanism through temperature-variable current density. Due to the advantage of a self-assembled monolayer (SAM) that can be obtained uniform molecular layer by simply placing devices in molecular solution, not only did it enable the production of functional molecular electronics devices but also allows us to study the characterization of the molecules. In addition, SAM can generate devices structure with nano-scale, three-dimensional (3-D) architectures. The point of non-vacuum, ambient temperature process of SAM can also generate molecular devices on flexible substrates. By using these strong point, we represented abnormal behavior of the rectifying molecules and reversible switching phenomena of diarylethene under flexible environment.

In chapter 2, we investigated charge transport mechanism of the rectifying type (ferrocne-alknaethiol) molecular devices both of rigid and flexible substrates. The rectifying molecular devices showed ~ 1.6 asymmetry value defined as different ratio of current density at both polarities ($\alpha \equiv \left| J(-1\ v)/J(+1\ V) \right|$). When compared to EGaIn junction with higher rectification ratio, the asymmetry value above is a very low, which is explained in the energy band diagram. The Fc HOMO level of ferrocen moiety, which has a significant effect on charge transport, located between Fermi level of each electrode (PEDOT:PSS and Au) at both polarities. Nevertheless, the reason of abnormal electrical behavior is understood to stand up configuration of alkly chain part and disordering of ferrocene moiety due to redox process. At about 0.6 volts in a cyclic voltammogram (CV), ferrocene moiety oxidized with ferrocenium cation ($Fc^{+2}$). The attractive force between the positively charged ferrocenium cation and the $SO_3^-$ part of PSS and the repulsive force between positive $Fc^{+2}$ and positively charged gold electrode leads to stand up the alkly chain part of rectifying molecules. From J-V data, we found that a different between ferrocene and ferrocenium is ~0.6 Å. In addition to this, the randomly repulsive force between each ferrocenium generate disordering, which makes contact poor with PEDOT:PSS interface. The redox process of ferrocene moiety occur at the positive bias, which can make different current density value between two polarities even small. To investigate electrical characterization of the rectifying molecular devices under mechanical deformation, we measured the

current density of three kind of molecular devices (FcC6, FcC8, FcC11) under bending condition. The molecular devices did not show remarkably current level changes and maintained abnormal current density behavior under several bending radii (10mm, 5mm) and a large number of repeated bending cycles.

In chapter 3, because of small asymmetry value we tried to find other types of molecules that can certainly show functionality. One of them, we fabricated the photoswitching molecular devices on flexible substrates and studied photoswitching characterization. The photoswitching is a kind of isomerization phenomenon and it has two electrical conductance states (high (closed) and low (open) conductance) by reacting with specific wavelength light form outside. Here, we show successfully the different in current density both two states and the conductance of closed states is higher than open. The electrical conductance discrepancy between to states is understood for the following three reasons. (1) connectivity and disconnectivity molecular orbitals by electrocylization (2) HOMO-LUMO level broadening defined as coupling constant Gamma (Γ) (3) length different of both two states by molecular dynamics simulation. To test photoswitching characterization of both states under physics strain, we measured the current density of both states under several bending radii (flat, 10 mm, 5 mm, 1 mm) and the repeated bending cycles (10, 100, 1000 times). The photoswitching molecular devices did not show seriously current level change and maintained the current density different of between closed and open states. The dominant charge transport mechanism of photoswitching molecules is

tunneling effect through temperature variable current density-voltage. The current density of two states did not change prominently when the temperature varied from 80 K to 300 K both two states. This results supported the fact that the charge transport mechanism of photoswitching molecules is tunneling effect.

In chapter 4, due to low transmittance of PEDOT:PSS/Au top electrode and low intensity of UV or visible light, we succeeded in showing the current level different between closed and open states, but did not show reversible photoswitching phenomena. To represent continuously reversible switching performance, we fabricated photoswitching molecular devices with reduced graphene oxide (rGO). The rGO have higher transmittance than PEDOT:PSS/Au and good conductivity (~ 3700 S/m). And Raman spectroscopy, XPS data indicate that rGO is enough to be used as top electrode. To use advantages of rGO top electrode, we examined the reversible photoswitching phenomenon in our molecular devices. The photoswitching devices showed reversibly switching between the two electrical states in response to the UV or visible light illumination. We measured the reversible photoswitching phenomenon several times by alternating between irradiation with a UV and a visible laser measured after fabricated and be stored for 30 days in ambient conditions. We were able to prove that the diarylethene molecular devices with an rGO top electrode exhibited a reliable and reversible photoswitching phenomenon in response to illumination.

# Bibliography


[1] A. von Hippel, *Science* **1956**, 123, 315.

[2] S. W. Herwald, S. J. Angello, *Science* **1960**, 132, 1127.

[3] A. Aviram, M. A. Ratner, *Chem. Phys. Lett*. **1974**, 29, 277.

[4] A. Aviram, Molecular Electronics-Science and Technology. Am. Inst. of Physics, New York, **1991**.

[5] R. R. Birge, Molecular, Biomolecular Electronics. *Am. Chem. Soc.* Washington, DC, **1991**.

[6] A. Ulman, An Introduction to Ultrathin Organic Films from Langmuir–Blodgett to Self-Assembly, Boston, CA: Academic Press **1991**.

[7] A. Nitzan. M. A. Ratner, *Science* **2003**, 300, 1384.

[8] J. R. Heath, M. A. Ratner, *Physics Today* **2003**, 56, 43.

[9] A. Salomon, D. Cahen, S. Lindsay, J. Tomfohr, V. B. Engelkes, C. D. Frisbie, *Adv. Mater.* **2003**, 15, 1881.

[10] M. A. Reed, T. Lee, Molecular Nanoelectronics, American Scientific, Stevenson Ranch, **2003**.

[11] R. L. McCreery, *Chem. Mater.* **2004**, 16, 4477.

[12] J. C. Love, L. A. Estroff, J. K. Kriebel, R. G. Nuzzo, G. M. Whitesides, *Chem. Rev.* **2005**, 105, 1103.

[13] D. K. Aswal, S. Lenfant, D. Guerin, J. V. Yakhmi, D. Vuillaume, *Anal. Chim. Acta* **2006**, 568, 84.

[14] R. Beckman, K. Beverly, A. Boukai, Y. Bunimovich, J. W. Choi, E. DeIonno, J. Green, E. Johnston-Halperin, Y. Luo, B. Sheriff, J. F. Stoddart, J. R. Heath, *Faraday Discuss.* **2006**, 131, 9.

[15] B. Ulgut, H. c. D. Abruňa, *Chem. Rev*. **2008**, 108, 2721.

[16] J. Zhang, A. M. Kuznetsov, I. G. Medvedev, Q. Chi, T. Albrecht, P. S. Jensen, J. Ulstrup, *Chem. Rev.* **2008**, 108, 2737.

[17] M. Galperin, M. A. Ratner, A. Nitzan, A. Troisi, *Science* **2008**, 319, 1056.

[18] H. Haick, D. Cahen, *Acc. Chem. Res*. **2008**, 41, 359.

[19] A. Vilan, O. Yaffe, A., Biller, A. Salomon, A. Kahn, D. Cahen, *Adv. Mater*. **2009**, 20,

[20] H. Choi, C. C. M. Mody, *Social Studies of Science* **2009**, 39, 11.

[21] R. L. McCreery, A. J. Bergren, *Adv. Mater*. **2009**, 21, 4303.

[22] L. Tao, H. Wenping, Z. Daoben, *Adv. Mater*. **2010**, 22, 286.

[23] J. C. Cuevas, E. Scheer, Molecular Electronics: An Introduction to Theory and Experiment, World Scientific Pub. Co. Inc, **2010**.

[24] H. Park, A. K. L. Lim, A. P. Alivisatos, J. Park, P. L. McEuen, *Appl. Phys. Lett.* **1999**, 75, 301.

[25] W. J. Liang, M. P. Shores, M. Bockrath, J. R. Long, H. Park, *Nature* **2002**, 417, 725.

[26] H. S. J. van der Zant, Y. -V. Kervennic, M. Poot, K. O'Neill, Z. de Groot, H. B. Heeersche, N. Stuhr-Hansen, T. Bjørnholm, D. Vanmaekelbergh, C. A. van Walree, L. W. Jenneskens, *Faraday Discuss.* **2006**, 131, 347.

[27] D. Natelson, L.H. Yu, J. W. Ciszek, Z.K. Keane, J.M. Tour, *Chem. Phys*. **2006**, 324, 267.

[28] H. Song, Y. Kim, Y. H. Jang, H. Jeong, M. A. Reed, T. Lee, *Nature* **2009**, 462, 1039.

[29] J. Moreland, J. W. Ekin, *J. Appl. Phys.* **1985**, 58, 3888.

[30] C. J. Muller, J. M. van Ruitenbeek, L. J. de Jongh, *Physica C* **1992**, 191, 485.

[31] R. Huber, M. T. Gonzalez, S. Wu, M. Langer, S. Grunder, V. Horhoiu, M. Mayor, M. R. Bryce, C. S. Wang, R. Jitchati, C. Schonenberger, M. J. Calame, *J. Am. Chem. Soc.* **2008**, 130, 1080.

[32] S. Wu, M. T. González, R. Huber, S. Grunder, M. Mayor, C. Schönenberger, M. Calame *Nat. Nanotech*. **2008**. 3. 569.

[33] M. T. González, S. Wu, R. Huber, S. J. van der Molen, C. Schönenberger, M. Calame, *Nano Lett.* **2006**, 6, 2238.

[34] E. Lörtscher, H. Weber, H. Riel, *Phys. Rev. Lett*. **2007**, 98, 176807.

[35] M. A. Reed, C. Zhou, C. J. Muller, T. P. Burgin, J. M. Tour, *Science* **1997**, 278, 252.

[36] J. van Ruitenbeek, E. Scheer, H. B. Weber, in: Lecture Notes in Physics: Introducing Molecular Electronics, Vol. 680 (Eds: G, Cuniberti, G, Fagas, K.Richter), Springer, Heidelberg, **2005**.

[37] J. Reichert, R. Ochs, D. Beckmann, H. B. Weber, M. Mayor, H. von Lohneysen, *Phys. Rev. Lett*. **2002**, 88, 176804.

[38] D. Djukic, J. M. van Ruitenbeek, *Nano Lett*. **2006**, 6, 789.

[39] J. H. Tian, B. Liu, X. L. Li, Z. L. Yang, B. Ren, S. T. Wu, N. J. Tao, Z. Q. Tian, *J. Am. Chem. Soc*. **2006**, 128, 14748.

[40] R. H. M. Smit, Y. Noat, C. Untiedt, N. D. Lang, M. C van Hemert, J. M. van Ruitenbeek, *Nature* **2002**, 419, 906.

[41] C. Kergueris, J. P. Bourgoin, S. Palacin, D. Esteve, C. Urbina, M. Magoga, C. Joachim, *Phys. Rev. B* **1999**, 59, 19.

[42] D. Dulic, S. J. van der Molen, T. Kudernac, H. T. Jonkman, J. J. D. de Jong, T. N. Bowden, J. van Esch, B. L. Feringa, B. J. van Wees, *Phys. Rev. Lett.* **2003**, 91, 207402.

[43] A. Aviram, M. A. Ratner, *Chem. Phys. Lett.* **1974,** 29, 277.

[44] C. A. Nijhuis, W. F. Reus and G. M. Whitesides, *J. Am. Chem. Soc.* **2009**, 131, 17814.

[45] J. G. Kushmerick, D. B. Holt, J. C. Yang, J. Naciri, M. H. Moore and R. Shashidhar, *Phys. Rev. Lett*. **2002**, 89, 086802.

[46] M. Elbing, R. Ochs, M. Koentopp, M. Fischer, C. von Hãnisch, F. Weigend, F. Evers, H. B. Weber, M. Mayor, *Proc. Natl. Acad. Sci*. **2005**, 102, 8815.

[47] I. Díez-Pérez, J. Hihath, Y. Lee, L. Yu, L. Adamska, M. A. Kozhushner, I. I. Oleynik and N. Tao, *Nature Chem*. **2009**, 1, 635.

[48] C. A. Nijhuis, W. F. Reus, A. C. Siegel, G. M. Whitesides, *J. Am. Chem. Soc.* **2011**, 133, 15397.

[49] C. A. Nijhuis, W. F. Reus, J. R. Barber, M. D. Dickey, G. M. Whitesides, *Nano Lett.* **2010**, 10, *3611*.

[50] C. A. Nijhuis, W. F. Reus, G. M. Whitesides, *J. Am. Chem. Soc.* **2010,** *132*, 18386.

[51] N. Nerngchamnong, L. Yuan, D. C. Qi, J. Li, D. Thompson, C. A. Nijhuis, *Nat. Nanotechnol*. **2013**, 8, 113.

[52] Y. Q. Liu, A. Offenhausser, D. Mayer, *Phys. Status Solidi A.* **2010,** *207*, 891.

[53] M. M. Thuo, W. F. Reus, C. A. Nijhuis, J. R. Barber, C. Kim, M. D. Schulz, G. M. Whitesides, *J. Am. Chem. Soc*. **2011**, 133, 2962.

[54] J. Chen, M. A. Reed, A. M. Rawlett, J. M. Tour, *Science* **1999**, 286, 1550.

[55] C. P. Collier, E. W. Wong, Belohradsk, yacute, M., F. M. Raymo, J. F. Stoddart, P. J. Kuekes, R. S. Williams, J. R. Heath, *Science* **1999**, 285, 391.

[56] E. Lörtscher, J. W. Ciszek, J. Tour, H. Riel, *Small*, **2006**, 2, 973.

[57] R. A. Bissell, E. Cordova, A. E. Kaifer, J. F. Stoddart, *Nature* **1994**, 369, 133.

[58] A. J. Kronemeijer, H. B. Akkerman, T. Kudernac, B. J. van Wees,B. L. Feringa, P. W. M. Blom, B. de Boer, *Adv. Mater*. **2008**, 20, 1467.

[59] W. Liang, M. P. Shores, M. Bockrath, J. R. Long, H. Park, *Nature* **2002**, 417, 725.

[60] J. Park, A. N. Pasupathy, J. I. Goldsmith, C. Chang, Y. Yaish, J. R. Petta, M. Rinkoski, J. P. Sethna, H. D. Abruna, P. L. McEuen, D. C. Ralph, *Nature* **2002**, 417, 722.

[61] D. R. Stewart, D. A. A. Ohlberg, P. A. Beck, Y. Chen, R. S. Williams, J. O. Jeppesen, K. A. Nielsen, J. F. Stoddart, *Nano Lett.* **2003**, 4, 133.

[62] J. E. Green, J. Wook Choi, A. Boukai, Y. Bunimovich, E. Johnston-Halperin, E. DeIonno, Y. Luo, B. A. Sheriff, K. Xu, Y. Shik Shin, H.-R. Tseng, J. F. Stoddart, J. R. Heath, *Nature* **2007**, 445, 414.

[63] M. A. Reed, J. Chen, A. M. Rawlett, D. W. Price, J. M. Tour, *Appl. Phys. Lett.* **2001**, 78, 3735.

[64] B. Behin-Aein, D. Datta, S. Salahuddin, S. Datta, *Nature Nanotech.* **2010**, 5, 266.

[65] J. Lee, H. Chang, S. Kim, G. S. Bang, H. Lee, *Angew. Chem. Int. Ed*. **2009**, 48, 8501.

[66] S. Seo, M. Min, S. M. Lee, H. Lee, *Nat. Commun.* **2013**, 4, 1920.

[67] M. Min, S. Seo, S. M. Lee, H. Lee, *Adv. Mater.* **2013**, 24, 7045.

[68] D. Kim, H. Jeong, H. Lee, W. T. Hwang, J. Wolf, E. Scheer, T. Huhn, H. Jeong, T. Lee, *Adv. Mater*. **2014**, 26, 3968.

[69] D. Kim, H. Jeong, W. T. Hwang, Y. Jang, D. Sysoiev, E. Scheer, T. Huhn, M. Min, H. Lee, T. Lee, *Adv. Funct. Mater*. **2015**, 25, 5918.

[70] M. Irie, *Chem. Rev*. **2000**, 100, 1685.

[71] M. Irie, T. Fukaminato, K. Matsuda, S. Kobatake, *Chem. Rev*. **2014**, 114, 12174.

[72] Y. Kim, T. J. Hellmuth, D. Sysoiev, F. Pauly, T. Pietsch, J. Wolf, A. Erbe, T. Huhn, U. Groth, U. E. Steiner, E. Scheer, *Nano Lett*. **2012**, 12, 3736.

[73] Y. Kim, G. Wang, M. Choe, J. Kim, S. Lee, S. Park, D. Y. Kim, B. H. Lee, T. Lee, *Organic Electronics* **2011**, 12, 2144.

[74] B. Xu, N. J. Tao, *Science* **2003**, 301, 1221.

[75] L. Venkataraman, J. E. Klare, C. Nuckolls, M. S. Hybertsen, M. L. Steigerwald, **Nature**, *2006*, 442, 904.

[76] P. Reddy, S.-Y. Jang, R. A. Segalman, A. Majumdar, *Science* **2007**, 315, 1568.

[77] S. Ho Choi, B. Kim, C. D. Frisbie, *Science* **2008**, 320, 1482.

[78] J. M. Beebe, B. Kim, J. W. Gadzuk, C. Daniel Frisbie, J. G. Kushmerick, *Phys. Rev. Lett.* **2006**, 97, 026801.

[79] T. D. Dumbar, M. T. Cygan, L. A. Bumm, G. S. McCarty, T. P. Burgin, W. A. Reinerth, L. Jones, J. J. Jackiw, J.

M. Tour, P. S. Weiss, D. L. Allara, *J. Phys. Chem. B*, **2000**, 104, 4880.

[80] L. Venkataraman, J. E. Klare, I. W. Tam, C. Nuckolls, M. S. Hybertsen, M. L. Steigerwald, *Nano Lett.* **2006**, 6, 458.

[81] H. Song, H. Lee, T. Lee, *Ultramicroscopy* **2008**, 108, 1196.

[82] J. G. Kushmerick, D. B. Holt, S. K. Pollack, M. A. Ratner, J. C. Yang, T. L. Schull, J. Naciri, M. H. Moore, R. Shashidhar, *J. Am. Chem. Soc.* **2002**, 124, 10654.

[83] J. G. Kushmerick, J. Naciri, J. C. Yang, R. Shashidhar, *Nano Lett*. **2003**, 3, 897.

[84] J. G Kushmerick, C. M. Whitaker, S. K. Pollack, T. L. Schull, R. Shashidhar, *Nanotechnology* **2004**, 15, S489.

[85] R. Haag, M. A. Rampi, R. E. Holmlin, G. M. Whitesides, *J. Am. Chem. Soc.* **1999**, 121, 7895.

[86] K. Slowinski, R. V. Chamberlain, C. J. Miller, M. Majda, *J. Am. Chem. Soc*. **1997**, 119, 11910.

[87] M. A. Rampi, O. J. A. Schueller, G. M. Whitesides, *Appl. Phys. Lett*. **1998**, 72, 1781-1783.

[88] K. Slowinski, H. K. Y. Fong, M. Majda, J. Am. Chem. Soc., 1999, 121, 7257.

[89] R. E. Holmlin, R. Haag, M. L. Chabinyc, R. F. Ismagilov, A. E. Cohen, A. Terfort, M. A. Rampi, G. M. Whitesides, *J. Am. Chem. Soc.* **2001**, 123, 5075.

[90] M. A. Rampi, G. M. Whitesides, *Chem. Phys*. **2002**, 281, 373.

[91] Grave, E. Tran, P. Samorì, G. M. Whitesides, M. A. Rampi, *Synth. Met*. **2004**, 147, 11.

[92] Duati, C. Grave, N. Tcbeborateva, J. Wu, K. Müllen, A. Shaporenko, M. Zharnikov, J. K. Kriebel, G. M. Whitesides, M. A. Rampi, *Adv. Mater*. **2006**, 18, 329.

[93] A. L. Harris, L. Rothberg, L. H. Dubois, N. J. Levinos, L. Dhar, *Phys. Rev. Lett*. **1990**, 64, 2086.

[94] R. Heinz, J. P. Rabe, *Langmuir* **1995**, 11, 506.

[95] A. Nemetz, T. Fischer, A. Ulman, W. Knoll, *J. Chem. Phys*. **1993**, 98, 5912.

[96] A. Dhirani, M. A. Hines, A. J. Fisher, O. Ismail, P. Guyot-Sionnest, *Langmuir*, **1995**, 11, 2609.

[97] P. Fenter, P. Eisenberger, J. Li, N. Camillone, S. Bernasek, G. Scoles, T. A. Ramanarayanan, K. S. Liang, *Langmuir* **1991**, 7, 2013.

[98] G. D. Aloisi, M. Cavallini, M. Innocenti, M. L. Foresti, Pezzatini, R. Guidelli, *J. Phys. Chem. B* **1997**, 101, 4774.

[99] M. Yu, S. M. Driver, D. P. Woodruff, *Langmuir* **2005**, 21, 7285.

[100] H. Rieley, G. K. Kendall, R. G. Jones, D. P. Woodruff, *Langmuir* **1999**, 15, 8856.

[101] M. Fonticelli, O. Azzaroni, G. Benitez, M. E. Martins, P. Carroand R. C. Salvarezza, *J. Phys. Chem. B*, **2004**, 108, 1898.

[102] D. Torres, P. Carro, R. C. Salvarezza, F. Illas, *Phys. Rev. Lett.* **2006**, 97, 226103.

[103] F. Schreiber, *Prog. Surf. Sci.* **2000**, 65, 151.

[104] O. Azzaroni, M. E. Vela, M. Fonticelli, G. Benı´tez, P. Carro, B. Blum, R. C. Salvarezza, *J. Phys. Chem. B* **2003**, 107, 13446.

[105] A. Imanishi, K. Isawa, F. Matsui, T. Tsuduki, T. Yokoyama, H. Kondoh, Y. Kitajima, T. Ohta, *Surf. Sci*. **1998**, 407, 282.

[106] H. Rieley, G. K. Kendall, A. Chan, R. G. Jones, J. Lu¨decke, D. P. Woodruff, B. C. C. Cowie, *Surf. Sci.* **1997**, 392, 143.

[107] J. C. Love, D. B. Wolfe, R. Haasch, M. L. Chabinyc, K. E. Paul, G. M. Whitesides, R. G. Nuzzo, *J. Am. Chem. Soc*. **2003**, 125, 2597.

[108] A. Carvalho,M. Geissler, H. Schmid, B. Michel, E. Delamarche, *Langmuir* **2002**, 18, 2406.

[109] H. Murayama, N. Ichikuni, Y. Negishi, T. Nagata, T. Tsukuda, *Chem. Phys. Lett.* **2003**, 376, 26.

[110] C. Majumder, *Langmuir* **2008**, 24, 10838.

[111] J. A. Williams, C. B. Gorman, *J. Phys. Chem. C*, **2007**, 111, 12804.

[112] G. Corthey, A. A. Rubert, G. A. Benitez, M. H. Fonticelli, R. C. Salvarezza, *J. Phys. Chem. C*, **2009**, 113, 6735.

[113] Z. Mekhalif, J. Riga, J. J. Pireaux, J. Delhalle, *Langmuir* **1997**, 13, 2285.

[114] S. Noeˆ l, F. Houze´, L. Boyer, Z. Mekhalif, J. Delhalle, R. Caudano, *IEEE Trans. Compon. Packag. Technol*. **1999**, 22, 79.

[115] M. E. Castro and J. M. White, *Surf. Sci.* **1991**, 257, 22.

[116] D. R. Mullins, T. Tang, X. Chen, V. Shneerson, D. K. Saldin, W. T. Tysoe, *Surf. Sci*. **1997**, 372, 193.

[117] C. J. Fisher, D. P. Woodruff, R. G. Jones, B. C. C. Cowie, V. Formoso, *Surf. Sci.* **2002**, 496, 73.

[118] Z.Mekhalif, F. Laffineur, N. Couturier, J. Delhalle, *Langmuir* **2003**, 19, 637.

[119] S. Bengio´, M. Fonticelli, G. Benı´tez, A. H. Creus, P. Carro, H. Ascolani, G. Zampieri, B. Blum, R. C. Salvarezza, *J. Phys. Chem. B* **2005**, 109, 23450.

[120] M. Rohwerder, M. Stratmann, *MRS Bull*. **1999**, 24, 43.

[121] C. Pirlot, J. Delhalle, J. J. Pireaux, Z. Mekhalif, *Surf. Coat. Technol.* **2001**, 138, 166.

[122] T. W. Kim, G. N. Wang, H. Lee, T. Lee, *Nanotechnology* **2007**, 18, 315204.

[123] G. Wang, T. W. Kim, H. Lee, T. Lee, *Phys, Rev, B* **2007**, 76, 205320.

[124] G. Wang, H. Yoo, S. I. Na, B. Cho, D. Y. Kim, T. Lee, *Thin Solid Films* **2009**, 518, 824.

[125] H. B. Akkerman, P. W. M. Blom, B. De Boer, *Nature* **2006**, 441, 69.

[126] P. A. Van Hal, E. C. P. Smits, T. C. T. Geuns, H. B. Akkerman, B. C. De Brito, S. Perissinotto, G. Lanzani, A. J. Kronemeijer, V. Geskinm J. Cornil, P. W. Blom, B. de Boer, D. M. de Leeuw, *Nat. Nanotechnol.* **2008**, 3, 7849.

[127] A. B. Neuhausen, A. Hosseini, J. A. Sulpizio, C. E. D. Chidsey, D. Goldhaber-Gordon, *Acs Nano* **2012**, 6, 9920.

[128] S. Park, G. Wang, B. Cho, Y. Kim, S. Song , Y. Ji, M. H. Yoon, T. Lee, *Nat. Nanotechnol.* **2012**, 7, 438.

[129] G. Wang, Y Kim, M. Choe, T. W. Kim, T. Lee, *Adv. Mater.* **2011**, 23, 755.

[130] S. Seo, M. Min, J. Lee, T. Lee, S. Y. Choi, H. Lee, *Angew. Chem. Int. Edit.* **2012**, 51, 108.

[131] H. Jeong, D. Kim, P. Kim, M. R. Cho, W. T. Hwang, Y. Jang, K, Cho, M. Min, D, Xiang, Y. D. Park, H. Jeong, T. Lee, *Nanotechnology* **2015**, 26, 025601.

[132] D. Tabor, *D. J. Colloid Interface Sci*. **1980**, 75, 240.

[133] B. Franklin, W. Brownrigg, Mr. Farish, *Phil. Trans. R. Soc*. **1774**, 64, 445.

[134] A. Pockels, *Nature* **1891**, 43, 437.

[135] A. Pockels, *Nature* **1892**, 46, 418.

[136] A. Pockels, *Nature* **1893**, 48, 15.

[137] A. Pockels, *Nature* **1894**, 50, 223.

[138] L. Rayleigh, *Phil. Mag.* **1899**, 50, 223.

[139] I. Langmir, *J. Am. Chem. Soc.* **1917**, 39, 1848.

[140] K. B. Blodgett, *J. Am. Chem. Soc*. **1935**,57, 1007.

[141] K. B. Blodgett, *Phys. Rev*. **1937**, 51,964.

[142] A. Tao, F. Kim, C. Hess, J. Goldberger, R. He, Y. Sun, Y. Xia, P. Yang, *Nano Lett.* **2003**, 3, 9, 1229.

[143] W. B. Yun, J. N. Bloch, *Rev. Sci. Instr.* **1989**, 60, 214.

[144] G. Haehner, C. Woell, M. Buck, M. Grunze, *Langmuir*, **1993**, 9, 1955.

[145] G. E. Poirier, *Chem. Rev*. **1977**, 97, 1117.

[146] A. Ulman, *Chem. Rev*. **1996**, 96, 1533.

[147] H. Jeong, D. Kim, G. Wang, S. Park, H. Lee, K. Cho, W. T. Hwang, M. H. Yoon, Y. H. Jang, H. Song, D. Xiang, T. Lee, *Adv. Funct. Mater*. **2014**, 24, 2472.

[148] R. G. Nuzzo, L. H. Dubois, D. L. Allara, *J. Am. Chem. Soc*. **1990**, 112, 558.

[149] R. G. Nuzzo, B. R. Zegarski, L. H. Dubois, *J. Am. Chem. Soc*. **1987**, 109, 733.

[150] M. W. Walczak, C. Chung, S. M. Stole, C. A. Widrig, M. D. Porter, *J. Am. Chem. Soc.* **1991**, 113, 2370.

[151] C. A. Widrig, C. Chung, M. D. Porter, *J. Electroanal. Chem*. **1991**, 310, 335.

[152] A. H. Schäfer, C. Seidel, L. Chi, H. Fuchs, *Adv. Mater*. **1998**, 10, 839.

[153] C. Boulas, J. V. Davidovits, F. Rondelez, D. Vuillaume, *Phys. Rev. Lett.* **1996**, 76, 4797.

[154] M. Fujihira, H. Inokuchi, *Chem. Phys. Lett*. **1972**, 17, 554.

[155] J. G. Simmons, *J. Appl. Phys*. **1963**, 34, 1793.

[156] J. G. Simmons, *J. Phys. D 4*, **1971**, 613.

[157] K. S. Novoselov, A. K. Geim, S. V. Morozov, D. Jiang, Y. Zhang, S. V. Dubonos, I. V. Grigorieva, A. A. Firsov, *Science* **2004**, 306, 666.

[158] I. Meric, M. Y. Han, A. F. Young, B. Ozyilmaz, P. Kim, K. L. Shepard, *Nat. Nanotechnol.* **2008**, 3, 654.

[159] Y. Zhang, J. W. Tan, H. L. Stormer, P. Kim, *Nature* **2005**, 438, 201.

[160] Q. H. Wang, M. C. Hersam, *Nat. Chem.* **2009**, 1, 206.

[161] H. Klauk, U. Zschieschang, J. Pflam, M. Halik, *Nature* **2007**, 445, 745.

[162] T. Sekitani, T. Yokota, U, Zschieschang, H Kluak, S. Bauer, K. Taekunchi, M. Takamiay, T. Sakurai, T. Someya, *Science* **2009**, 326, 1516.

[163] G. H. Gelinck, H. E. A. Huitema, E. van Veenendaal, E. Cantatore, L. Schrijnemakers, Jan B. P. H. van der Putten, T. C. T. Geuns, M. Beenhakkers, J. B. Giesbers, B. H. Huisman, E. J. Meijer, E. M. Benito, F. J. Touwslager, A. W. Marsman, B. J. E. van Rens, D. M. de Leeuw, *Nature Materials* **2004**, 3, 106.

[164] L. G. D. Arco, Y. Zhang, C. W. Schlenker, K. Ryu, M. E. Thompson, C. Zhou, *ACS Nano*, **2010**, 4, 2865.

[165] D. H. Kim, J. Viventi, J. J. Amsden, J Xiao, L. Vigeland, Y. S. Kim, J. A. Boanco, B. Panilaitis, E. S. Frechette, D. Contreras, D. L. Kaplan, F. G. Omenetto, Y. Huang, K. C. Hwang, M. R. Zakin, B. Litt, J. A. Rogers, *Nature Materials* **2010**, 9, 511.

[166] S. Ye, Y, Sato, K. Uosaki, Langmuir 1997, 13, 3157.

[167] S. Ye, T, Haba, Y. Sato, K. Shimazu, K. Uosaki, *Phys. Chem. Chem. Phys*. **1999**, 1, 3653.

[168] H. Jeong, Y. Jang, D. Kim, W. T. Hwang, J. W. Kim, T. Lee, *J. Phys. Chem. C.* **2016**, 120, 3564.

[169] S. Seo, M. Min, J. Lee, S. Y. Choi, H. Lee, *Angew. Chem. Int. Ed.* **2012**, 41, 108.

[170] H. Zhang, E. Bekyarova, J. W. Huang, Z. Zho, W. Bao, F. Wang, R. C. Haddon, C. N. Lau, *Nano Lett*. **2011**, 11, 407.

[171] A. C. Ferrari, J. C. Meyer, V. Scardaci, C. Casirashi, M. Lazzeri, F. Mari, S. Piscanec, D. Jiang, K. S. Novoselov, S. Roth, A. K. Geim, *Phys. Rev. Lett*. **2006**, 97, 187401.

[172] E. Bekyarova, M. E. Itkis, P. Ramesh, C. Berge, M. Sprinkle, W. A. de Heer, R. C. Haddon, *J. Am. Chem. Soc*. **2009**, 131, 1336.

[173] D. R. Dreyer, S. Park, C. W. Bielawski, R. S. Ruoff, *Chem. Soc. Rev*. **2010**, 39, 228.

# Appendix A

## Self-assembled monolayer

In chapter 1, we introduced self-assembly method that deposit molecules on substrates. We handled in earnest about chemisorption between thiol end group and gold bottom electrode. The monothiol and dithiol which are kind of thiol group have slightly different deposition process on interface of gold.

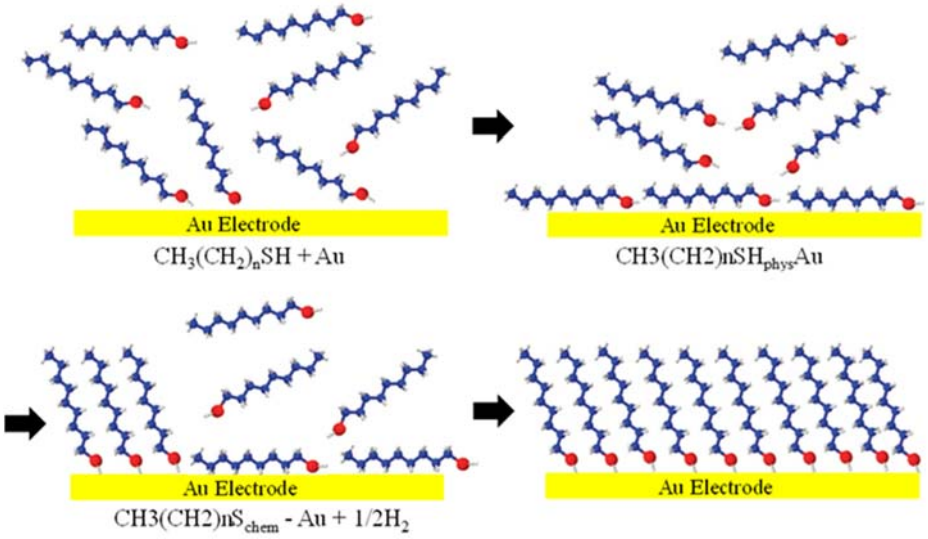


**Figure A. 1. The process of self-assembled monolayer between monothiol and gold surface**

In case of thiol as shown figure A 1, when substrate is dipped onto molecular solution, molecules combine with interface particle of gold electrode by physisorption, lying down phase itself. Next, molecules chemisorb on interface of gold particles through sulfur with strongly covalent bond, losing hydrogen atom. Unfortunately, it have been not understood fully thee process of changing from physisorption to chemisorption and losing hydrogen atom.

Some hypotheses have been suggested such as redox reactions. And then, the molecules lying down on surface begin to take place by van der Waals force between neighborhood molecules. After substrates is dipped onto molecular solution for 24-48 h, we can obtain well-formed molecular layer on substrates.

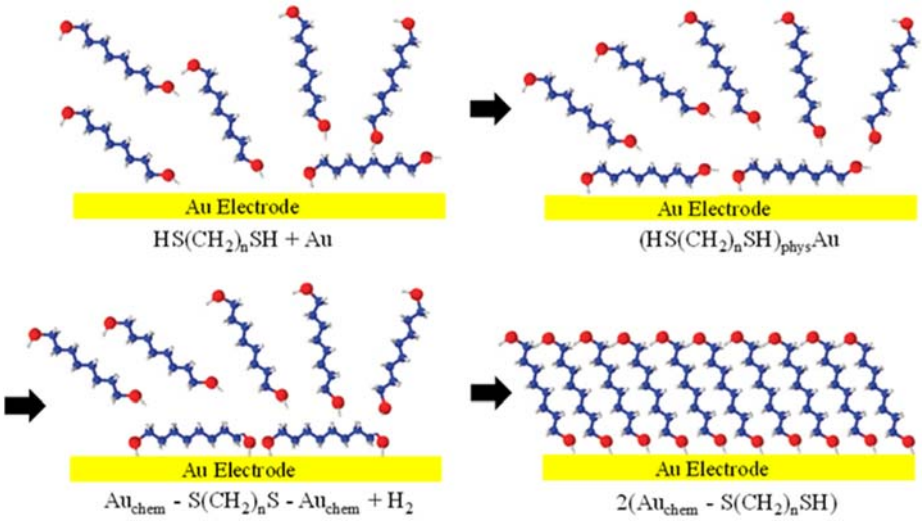


**Figure A. 2. The process of self-assembled monolayer between dithiol and gold surface**

In other case of dithiol, even though dithiol has similar process of SAM compared with thiol, both side of sulfur chemisorption with gold surface particles because both side are composed of sulfur in the third step as shown figure B. 2. At this step, the other dithiol molecules free one side of chemisorbed molecules thus two molecules can be standing up which can be written by Au-S-$(CH_2)_n$S-Au + $HS(CH_2)_nSH$ -> 2[Au-S$(CH_2)_n$SH]. Since the dithiol chemisorbed between both end side of sulfur and surface materials, it has possibility of difficult of obtaining well-formed molecular layer, compared with thiol. Among the molecules used in this theses, alknaethiol and ferrocene-

alknaethiol(rectifying) are monothiol type molecule while diarylethene (photoswitching) is dithiol one.

# Appendix B

## Mechanism of photoswitching molecule

In the chapter 3 and 4, we introduced photoswitching diarylethene class molecules with PEDOT:PSS/Au or reduced graphene oxide(rGO), respectively. The mechanism of switching can be explained by pericyclic reaction of organic chemistry. Specifically, because the switching part of molecules is composed of six carbons which appear alternately single or double bond, it can be rearranged by reacting outside light energy through electrocyclization as shown figure B. (b).

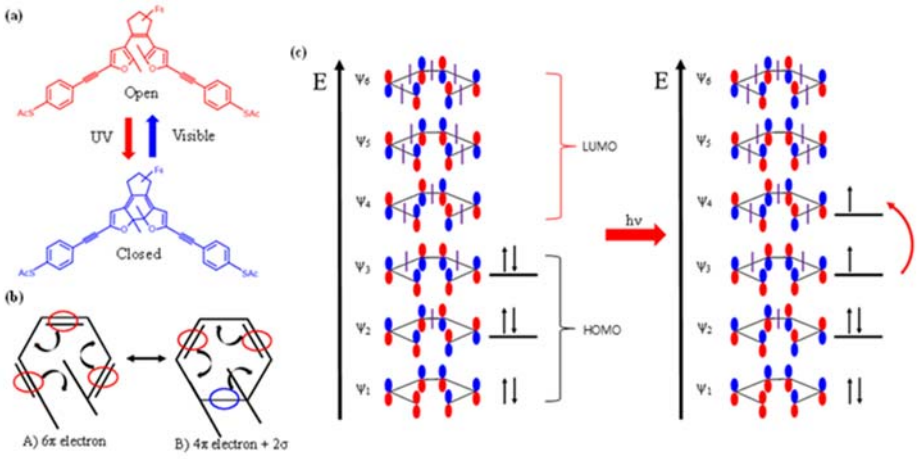


**Figure B. 1. (a) Chemical structure of photoswitching molecules (b) Switching part of photoswitching molecules (c) Diarylethene 6π molecular orbitals**

When we consider HOMO-LUMO states of switching part of diarylethene like figure B. (c), a one electron at $\Psi_3$ is transferred to exited state $\Psi_4$, being received light energy from outside. Then, according to Woodward-Hoffmann rules, the outermost $P_z$ orbitals on both of end carbon rotates to create a sigma-bond which can electrically shared. Since existing broken part change into a bond that electron can pass through, the conductance of closed state is supposed to lead to higher than open state.

국문초록

# 정류 분자 소자와 광스위칭 분자 소자의 전기적 특성 연구

분자전자소자 연구 분야는 정류소자, 트랜지스터, 메모리, 광스위칭과 같은 많은 실험 분야에서 다양하게 연구되고 있다. 자기조립단분자막(self-assembled monolayer, SAM)방식은 기능성 분자를 소자의 한 구성요소로 사용할 수 있게 해주었고 이는 저비용, 고효율, 낮은 열전도율, 소자의 소형화와 같은 장점을 가지게 해주었다. 그러나, 초창기의 분자전자소자는 상단 전극이 분자층 사이로 침투하면서 전기적 단락(electrical short)현상으로 인하여 소자 자체의 수율(yield)이 굉장히 낮은 (~1 %) 심각한 문제를 가지고 있었다. 소자 자체의 저수율 문제를 해결하기 위해서 몇 가지 방법들이 제시되었는데, 전도성 고분자 혹은 그래핀 필름과 같은 내부부호층을 분자층과 상단 전극 사이에 넣어주는 것이다. 혹은 상단 전극을 분자층 위로 직접 전수해주는 방법도 개발되었다. 결과적으로 이러한 방식들은 분자전자소자의 수율을 높여 주었고(~80 %) 소자 자체의 성능도 긴 시간 동안 유지할 수 있게 해 주었다.

고수율 분자소자를 만들 수 있게 됨으로써 소자를 심지어 유연한 기판 위에서도 제작 가능하게 되었다. 기존에 alknaethiol

분자를 유연한 기판 위에 분자전자소자로 제작하고 그 전기적 특성을 기판의 물리적 변형 조건에서 연구하였다. 그러나, alknaethiol 분자는 소자 자체에 기능성을 주지 못하는 절연체 분자이기 때문에 실제적인 기능성 소자로의 직접적인 적용은 어렵다. 따라서 소자 기능성을 가지는 분자전자소자를 유연한 기판 위에 제작하는 것이 중요하다. 본 학위 논문에서는 기능성 분자인 정류 분자(rectifying)와 광스위칭(photoswitching) 분자를 유연한 기판 위에 제작하고 기판의 물리적 변형 조건에서 그 전기적 특성에 대해서 연구하였다. 첫번째 기능성 분자로서 ferrocene-alknaethiolate 분자전자소자를 실리콘 기판과 유연한 기판 위에 제작하여 그 특성을 연구한 결과, 양과 음의 전압에서 비대칭 전류 값을 가지는 전기적 특성을 일관되게 보여주었다. 비록 비대칭 전류 비율은 약 1.6 정도로 높진 않았지만, 이러한 비대칭 전류 특성은 ferocene 부분의 산화 환원 반응에 의한 것으로 설명이 가능하였다. 특히 이 정류 분자전자소자는 물리적인 변형 조건에서도 비대칭 전기적 특성을 잘 유지하였다. 두번째 기능성 분자로서 diarylethene 분자는 두 가지의 전기적 상태를 가지는 것으로 알려져 있다. diarylethene 분자에서는 닫힌(높은 전도도) 상태와 열린(낮은 전도도) 상태가 자외선(UV) 혹은 가시광선과 반응하여 생성된다. 이러한 두 전기적 상태는 소자 제작과정에서 UV 혹은 가시광선에 독립적으로 노출되어 두 상태가 정해졌으며 두 상태의 전류 값이 차이가 나는 것을 보였다. 그러나 소자제작이 완성된

diarylethene 분자소자는 가역적인 스위칭 현상을 보여주지는 못하였다. 마지막으로, 가역적인 광스위칭 현상을 구현하기 위해서 환원된 산화 그래핀(reduced graphene oxide, rGO)를 상단 전극으로 사용하여 diarylethene 분자전자소자를 제작하고 그 특성을 연구하였다. rGO 전극을 사용한 광스위칭 분자전자소자는 뚜렷하게 두 전기적 상태의 전류 값이 차이가 나는 것과 특히 가역적인 스위칭 현상이 구현되었다. 본 학위 논문에서는 유연한 기판 위에서 기능성 분자 전자 소자의 제작이 가능하다는 것을 보여주었다.

**주요어**: 분자전자소자, 자기조립단분자막, 고수율 분자소자, 정류현상, 산화 환원 반응, 이성질화, 환원된 산화 그래핀, 플렉시블 전자회로

**학번**: 2010-20358